

Azimuth moveout for 3-D prestack imaging

Biondo Biondi, Sergey Fomel, and Nizar Chemingui

Stanford Exploration Project, 360 Mitchell Bldg., Stanford, CA 94305-2215

(July 30, 1997)

ABSTRACT

We introduce a new partial prestack-migration operator, named azimuth moveout (AMO), that rotates the azimuth and modifies the offset of 3-D prestack data. Followed by partial stacking, AMO can reduce the computational cost of 3-D prestack imaging. We have successfully applied AMO to the partial stacking of a 3-D marine data set over a range of offsets and azimuths. When AMO is included in the partial-stacking procedure, high-frequency steeply-dipping energy is better preserved than when conventional partial-stacking methodologies are used. Because the test data set requires 3-D prestack depth migration to handle strong lateral variations in velocity, the results of our tests support the applicability of AMO to prestack depth-imaging problems.

AMO is a partial prestack-migration operator defined by chaining a 3-D prestack imaging operator with a 3-D prestack modeling operator. The analytical expression for the AMO impulse response is derived by chaining constant-velocity DMO with its inverse. Equivalently, it can be derived by chaining constant-velocity prestack migration and modeling. Because 3-D prestack data are typically irregularly sampled in the surface coordinates, AMO is naturally applied as an integral operator in the time-space domain. The AMO impulse response is a skewed saddle surface in the time-midpoint space. Its shape depends on the amount of azimuth rotation and offset continuation to be applied to the data. The shape of the AMO saddle is velocity independent, whereas its spatial aperture is dependent on the minimum velocity.

When the azimuth rotation is small ($\leq 20^\circ$), the AMO impulse response is compact and its application as an integral operator is inexpensive. Implementing AMO as an integral operator is not straightforward because the AMO saddle may have a strong curvature when it is expressed in the midpoint coordinates. An appropriate transformation of the midpoint axes to regularize the AMO saddle leads to an effective implementation.

INTRODUCTION

To improve the accuracy and reduce the cost of 3-D prestack imaging, it can be useful to modify the effective azimuth and offset distribution of the data during processing without detailed a priori assumptions about the underlying velocity function or geology. In this paper, we introduce a partial prestack-migration operator that rotates the data's azimuth and changes the data's absolute offset. Because of its ability to modify the azimuth of the data, we named this operator azimuth moveout (AMO).

There are many potential applications for the AMO operator. In this paper we discuss its application to partial stacking of 3-D data before prestack migration. We show that the application of AMO significantly improves, with respect to conventional methods, the result of partial stacking of a 3-D marine data set over a range of offsets and azimuths. Partial stacking reduces the cost of 3-D prestack imaging by reducing the amount of data to be migrated (Hanson and Witney, 1995), because the cost of migration is approximately proportional to the amount of data to be migrated. However, for partial stacking to enhance reflections and suppress noise, reflections need to be coherent across the traces to be stacked. Normal moveout (NMO) increases the coherency of reflections over offsets by a first-order correction of their traveltime. Therefore, NMO is often applied to traces before partial stacking (Hanson and Witney, 1995). However, a simple trace-to-trace transformation such as NMO is insufficient

when the reflections have conflicting dips or diffractions occur. By correctly moving the dipping energy across midpoints, AMO insures the preservation of all dips in the data during partial stacking. In preserving dipping energy during the stacking process AMO is analogous to DMO, but the two processes substantially differ in the nature of their respective output. DMO transforms prestack data into equivalent zero-offset data that cannot be properly imaged by prestack depth migration. In contrast, AMO transforms prestack data into equivalent not-zero-offset data that can be used as input to prestack depth migration.

For reducing the computational cost of prestack migration, an alternative to partial stacking is to migrate only a subset of the available traces. To minimize the effects of data aliasing caused by the data subsampling, the input traces can be selected according to a quasi-random selection criterion (Zhou and Schuster, 1995). This method can be attractive in high signal-to-noise areas when all the data offsets are stacked during migration. However, when the signal-to-noise ratio is low, and/or when a prestack analysis of migration results is desired, either for velocity estimation or for AVO purposes, partial stacking is more robust with respect to noise, either coherent or incoherent, because it uses all the available traces to improve the signal-to-noise ratio. A combination of the two methods, that is, the synthesis by AMO and partial stacking of a quasi-randomly sampled data set, has the potential of reducing the cost of imaging even further, but its testing is beyond the scope of this paper.

AMO can be considered a generalization of dip moveout (DMO) (Deregowski and Rocca, 1981; Hale, 1984), in the sense that it transforms prestack data into equivalent data with an arbitrary offset and azimuth; in contrast, DMO is only capable of transforming non zero-offset data to zero-offset data. AMO is derived by analytically evaluating the operator that is equivalent to the the chain of a 3-D prestack imaging operator with the corresponding 3-D prestack modeling. Any 3-D prestack imaging operator can be used for defining AMO. However, our analytical closed-form expression for AMO was derived only by use of constant-velocity DMO and constant

velocity prestack migration and modeling. Goldin (1994) and Hubral et al. (1996) have recently presented a very general theory for chaining imaging operators; however the implementation of their theory would require an expensive numerical evaluation of the chained operators. The derivation of AMO from constant-velocity operators has the further advantage of making the kinematics of the operator velocity-independent. Notwithstanding the constant-velocity assumption underlying its derivation, AMO can be effectively applied to data recorded from a complex velocity model, as the data example in this paper demonstrates. The first-order effects of velocity variations are removed by NMO, which is applied before AMO, as it is also usually assumed when applying DMO. However, AMO can successfully transform data to nearby offsets and azimuths, when velocity variations are too strong for DMO to transform data correctly all the way to zero-offset. Because AMO is correct to the first order, its results are accurate if the amounts of azimuth rotation and offset continuation are sufficiently small.

In addition to the data-reduction application presented in this paper, the AMO operator has a wide spectrum of potential applications in the processing of 3-D seismic data. A promising application is the transformation of narrow-azimuth marine surveys to effective common-azimuth data. Common-azimuth data can be efficiently depth-imaged by new 3-D prestack migration methods (Canning and Gardner, 1996b; Biondi and Palacharla, 1996), when the underlying assumptions of these methods are satisfied. AMO can also improve the amplitude accuracy of prestack imaging wide-azimuth data recorded with irregular geometry by applying it before full prestack imaging to regularize the data geometry (Chemingui and Biondi, 1996). For some applications, such as the synthesis of 2-D lines from 3-D data, AMO is related to the 3-D data regularization method proposed by Canning and Gardner (1996a), which is based on the successive application of DMO and inverse DMO. However, AMO can be applied to a wider set of problems and data sets because the geometry of the output data is not constrained to be common-azimuth. Therefore, in addition to transform-

ing marine surveys to effective common-azimuth data, AMO can be applied to more general data-regularization problems, as well as to data reduction and interpolation. Furthermore, the application of AMO as a single-step procedure has two benefits: substantial computational savings because of the small size of the AMO operator when azimuth rotation and offset continuation are small, and simplified handling of large data sets because one less pass through the data is required.

The next section introduces the AMO operator and analyzes the characteristics of the AMO impulse response. The second section introduces a transformation of the midpoint coordinates that is important to an efficient and accurate implementation of AMO as an integral operator. Finally, the third section of the paper presents the results obtained when AMO was applied to the partial stacking of a 3-D marine survey. The appendices contain the derivations of the main analytical results; that is, the expressions for the kinematics, the amplitudes, and the aperture extent of the AMO impulse response.

AMO OPERATOR

We define AMO as an operator that transforms 3-D prestack data with a given offset and azimuth to equivalent data with different offset and azimuth. To derive the AMO operator we collapse into one single step the sequence of an imaging operator and a forward modeling operator. In principle, any 3-D prestack imaging operator can be used for defining AMO. We initially chained DMO and “inverse” DMO, but, to derive an accurate expression for the spatial aperture of AMO, we had to use full 3-D prestack constant-velocity migration and its inverse. As expected, the kinematics of AMO are independent from its derivation.

AMO is not a single-trace to single-trace transformation, but it is a partial-migration operator that moves events across midpoints according to their dip. Its impulse response is a saddle in the output’s midpoint domain. The shape

of the saddle depends on the offset vector of the input data $\mathbf{h}_1 = h_1 \cos \theta_1 \mathbf{x} + h_1 \sin \theta_1 \mathbf{y} = h_1(\cos \theta_1, \sin \theta_1)$ and on the offset vector of the desired output data $\mathbf{h}_2 = h_2(\cos \theta_2, \sin \theta_2)$, where the unit vectors \mathbf{x} and \mathbf{y} point respectively in the in-line direction and the cross-line direction. The time shift to be applied to the data is a function of the difference vector $\Delta \mathbf{m} = \Delta m(\cos \Delta \varphi, \sin \Delta \varphi)$ between the midpoint of the input trace and the midpoint of the output trace. The analytical expression of the AMO saddle, as derived in Appendices A and B, is

$$t_2(\Delta \mathbf{m}, \mathbf{h}_1, \mathbf{h}_2, t_1) = t_1 \frac{h_2}{h_1} \sqrt{\frac{h_1^2 \sin^2(\theta_1 - \theta_2) - \Delta m^2 \sin^2(\theta_2 - \Delta \varphi)}{h_2^2 \sin^2(\theta_1 - \theta_2) - \Delta m^2 \sin^2(\theta_1 - \Delta \varphi)}}. \quad (1)$$

The traveltimes t_1 and t_2 are respectively the traveltime of the input data after NMO has been applied, and the traveltime of the results before inverse NMO has been applied.

The surface represented by equation (1) is a skewed saddle; its shape and spatial extent are controlled by the values of the absolute offsets h_1 and h_2 , and by the azimuth rotation $\Delta \theta = \theta_1 - \theta_2$ (Figure ??). Consistent with intuition, the spatial extent of the operator has a maximum for rotation of 90 degrees, and it vanishes when offsets and azimuth rotation tend to zero. Furthermore, it can be easily verified that $t_2 = t_1$ for the zero-dip components of the data; that is, the kinematics of zero-dip data after NMO do not depend on azimuth and offset.

The expression for the kinematics is velocity independent, but the lateral aperture of the operator is velocity dependent. An upper bound on the spatial extent of the AMO operator is defined by the region where the expression in equation (1) is valid. Equation (1) becomes singular when

$$\frac{|\Delta \mathbf{m} \times \mathbf{h}_1|}{|\mathbf{h}_1 \times \mathbf{h}_2|} = 1, \quad (2)$$

or

$$\frac{|\Delta \mathbf{m} \times \mathbf{h}_2|}{|\mathbf{h}_1 \times \mathbf{h}_2|} = 1. \quad (3)$$

The geometric interpretation of these conditions is that the support of the AMO operator is limited to the region within the parallelogram with main diagonal $(\mathbf{h}_1 + \mathbf{h}_2)$ and minor diagonal $(\mathbf{h}_1 - \mathbf{h}_2)$. The shaded area in Figure 2 shows an example parallelogram that represents the maximum possible spatial extent of the AMO operator. More stringent bounds for the AMO aperture can be derived (Appendix C) by imposing the condition that the reflector dip must be equal or less than 90° . These bounds are, for given \mathbf{h}_1 and \mathbf{h}_2 , functions of the minimum velocity V_{min} and of the input traveltimes. The parallelogram in Figure 2 is thus the worse case, when either the velocity or the input traveltimes is equal to zero. Figure ?? shows the effective AMO impulse response when the velocity-dependent aperture limitation, corresponding to a realistic minimum velocity of 2 km/s, is applied to the impulse response shown in Figure ?. The surface shown in Figure ? is significantly narrower than the whole impulse response shown in Figure ?. This velocity-dependent aperture limitation is important for an efficient use of AMO and it contributes to make the cost of applying AMO to the data small compared to the cost of applying a full 3-D prestack migration.

The smaller is the azimuth rotation $\Delta\theta$, the smaller the effective aperture becomes. At the limit, the expression in equation (1) is singular when the azimuth rotation vanishes and the AMO surface reduces to a 2-D line. This 2-D operator, corresponding to the case of *offset continuation* (Bolondi et al., 1984), has been derived independently by Biondi and Chemingui (1994), Stovas and Fomel (1996), and (in a different form) by Bagaini et al. (1994). It is given by the following quadric equation,

$$\begin{aligned}
& t_2(\Delta m, h_1, h_2, t_1) = \\
& \frac{t_1 \sqrt{(h_1^2 + h_2^2) - \Delta m^2 + \sqrt{[(h_1 - h_2)^2 - \Delta m^2][(h_1 + h_2)^2 - \Delta m^2]}}}{\sqrt{2}h_1} h_2 \geq h_1 \\
& \frac{t_1 \sqrt{(h_1^2 + h_2^2) - \Delta m^2 + \sqrt{[(h_1 - h_2)^2 - \Delta m^2][(h_1 + h_2)^2 - \Delta m^2]}}}{\sqrt{2}h_2} h_2 \leq h_1.
\end{aligned} \tag{4}$$

The apparent dichotomy between the 3-D and the 2-D solutions is reconciled when

the effective aperture of the AMO operator is taken into account; Fomel and Biondi (1995a) showed that the 3-D operator monotonously shrinks to a line, and the limit of the kinematics of the 3-D operator [equation (1)] approaches the 2-D operator [equation (4)].

While the kinematics of AMO are independent from its derivation, the amplitude term varies according to the derivation. For the AMO applications presented in this paper, we used the AMO amplitude that is related to Zhang-Black DMO (Zhang, 1988; Black et al., 1993). It can be shown that the choice of the Zhang-Black's Jacobian yields an amplitude-preserving AMO operator, at least when applied on regularly sampled common offset-azimuth cubes (Chemingui and Biondi, 1995). This particular choice of the Jacobian results in the following amplitude term:

$$A(\Delta \mathbf{m}, \mathbf{h}_1, \mathbf{h}_2, t_2) \approx \frac{|\omega_2| t_2}{2 \pi h_1 h_2 \sin \Delta \theta} \frac{1 + \frac{\Delta m^2 \sin^2(\theta_2 - \Delta \varphi)}{h_1^2 \sin^2 \Delta \theta}}{\left(1 - \frac{\Delta m^2 \sin^2(\theta_2 - \Delta \varphi)}{h_1^2 \sin^2 \Delta \theta}\right) \left(1 - \frac{\Delta m^2 \sin^2(\theta_1 - \Delta \varphi)}{h_2^2 \sin^2 \Delta \theta}\right)}. \quad (5)$$

Notice that the frequency $|\omega_2|$ enters as multiplicative factor in the expression for AMO amplitudes. This term can be applied to the output data in the time domain by chaining a causal half-differentiator with an anti-causal half-differentiator.

INTEGRAL IMPLEMENTATION OF AMO

One of the main advantages of AMO is that it is a narrow operator and that consequently its application to a full 3-D prestack data set is much less costly than the application of full 3-D prestack migration. However, designing an accurate and efficient implementation of the AMO operator is not straightforward. Therefore, in this section we discuss the issues relevant to an effective implementation of the AMO process, as defined in the previous sections. The main challenge is to devise an efficient method that avoids operator aliasing and simultaneously takes advantage of

the opportunity for saving computation, by properly limiting the spatial extent of the numerical integration.

The AMO integration surface has the shape of a saddle. The exact shape of the saddle depends on the azimuth rotation and offset continuation that are applied to the input data. When the azimuth rotation is small, the saddle has a strong curvature. Conventional anti-aliasing methods (Gray, 1992; Bevc and Claerbout, 1992; Lumley et al., 1994) are based on an adaptive low-pass filtering of the data as a function of the operator local dips. When there is a strong curvature, the dips change too quickly for a simple low-pass filter of the input trace to both suppress the aliased dips *and* preserve the non-aliased dips. To address this problem, we perform the spatial integration in a transformed coordinate system. In this new coordinate system, the AMO surface is well behaved, and its shape is invariant with respect to the amount of azimuth rotation and offset continuation.

Transformation of midpoint axes

The appropriate midpoint-coordinate transformation to be applied to the AMO impulse response is described by the following chain of transformations

$$\begin{bmatrix} \xi_1 \\ \xi_2 \end{bmatrix} = \begin{bmatrix} \frac{1}{h_2 \sin \Delta\theta} & 0 \\ 0 & \frac{1}{h_1 \sin \Delta\theta} \end{bmatrix} \begin{bmatrix} -\sin \theta_1 & \cos \theta_1 \\ -\sin \theta_2 & \cos \theta_2 \end{bmatrix} \begin{bmatrix} \Delta m_x \\ \Delta m_y \end{bmatrix}, \quad (6)$$

where ξ_1 , and ξ_2 are the transformed midpoint coordinates. Figure 4 shows a schematic of the relationship between the input and output offset vectors \mathbf{h}_1 and \mathbf{h}_2 , and the transformed midpoint-coordinate unit vectors ξ_1 and ξ_2 . Notice that the ξ axes are dual with respect to \mathbf{h}_1 and \mathbf{h}_2 , but they define a new coordinate system for the midpoint axes of the AMO operator. The right matrix in equation (6) represents a space-invariant rotational squeezing of the coordinate, while the left matrix is a simple rescaling of the axes by a factor dependent on the azimuth rotation $\Delta\theta$, and by the length of the dual offset vectors. When the azimuth rotation is zero, the

transformation described in equation (6) becomes singular. In this case the AMO operator degenerates into the 2-D offset continuation operator, as discussed in a previous section. In practice, a simple pragmatic method to avoid the singularity is to set a lower limit for the product $h_1 h_2 \sin(\Delta\theta)$. Because the 3-D AMO operator converges smoothly to the 2-D offset continuation operator (Fomel and Biondi, 1995b), the error introduced by this approximation is negligible.

In this new coordinate system, the kinematics of AMO are described by the following simple relationship between the input time t_1 and the output time t_2 :

$$t_2(\xi_1, \xi_2) = t_1 \sqrt{\frac{1 - \xi_2^2}{1 - \xi_1^2}}, \quad (7)$$

and the amplitudes (based on Zhang-Black amplitudes for DMO) are described by the following equation

$$A(\xi_1, \xi_2) = \frac{t_2 |\omega_2|}{2\pi} \frac{(1 + \xi_1^2)}{(1 - \xi_1^2)(1 - \xi_2^2)}. \quad (8)$$

This expression for the amplitudes takes into account the Jacobian of the transformation described in equation (6).

Operator antialiasing

The AMO operator can be steeply dipping, and thus antialiasing is critical to produce high-quality results. To apply antialiasing, we use a simple low-pass filtering of the input trace with a bandwidth that varies spatially along the operator and is a function of the local time dips of the operator. The time dips can be computed analytically according to the following equations:

$$\frac{\partial t_2}{\partial \xi_1} = t_2 \frac{\xi_1}{1 - \xi_1^2}, \quad (9)$$

and

$$\frac{\partial t_2}{\partial \xi_2} = -t_2 \frac{\xi_2}{1 - \xi_2^2}. \quad (10)$$

Operator aperture

Expressions (7) and (8) for the kinematics and amplitudes of AMO are valid for ξ_1 and ξ_2 ranging between -1 and 1 . However, for finite propagation velocities, the AMO operator has a much narrower aperture, as shown in Appendix C. Taking into account this finite aperture is crucial both for accuracy and for efficiency. For a given minimum propagation velocity V_{min} , the maximum output time can be evaluated according to the following condition:

$$\gamma_1 = \frac{\frac{\partial t_2}{\partial \xi_1}}{t_2 h_2 \sin \Delta\theta} , \quad (11)$$

$$\gamma_2 = -\frac{\frac{\partial t_2}{\partial \xi_2}}{t_2 h_1 \sin \Delta\theta} , \quad (12)$$

and

$$t_2 \leq \frac{2}{V_{min} \sqrt{(\gamma_1^2 + \gamma_2^2 - 2\gamma_1\gamma_2 \cos \Delta\theta) (1 - \xi_1^2)}} . \quad (13)$$

To avoid truncation artifacts a tapering function is used at the edges of the operator aperture.

APPLICATION OF AMO TO A 3-D MARINE DATA SET

This section presents the results of applying AMO prior to partial stacking, to a marine data set recorded in the North Sea. We compare the results of partial stacking after NMO and AMO, with the results of partial stacking after simple NMO. The results show that adding AMO to the processing sequence better preserves the steeply dipping energy in the partially-stacked data. The partially-stacked data are still in the prestack domain; that is they are equivalent to data recorded at not-zero offset. This is important, because the goal of partial stacking is to reduce the cost of the subsequent 3-D prestack depth migration. Therefore, the results of partial stacking after AMO cannot be directly compared with the results of partial stacking after DMO, that transforms data to zero offset.

The data set is a valuable test case for AMO because it shows numerous fault diffractions and because proper imaging of it requires 3-D prestack depth migration (Hanson and Witney, 1995). Figure 5 shows an in-line geological section of the area of the survey and the respective velocities of the layers. Figure 6 shows a common-offset in-line section of the data set, at the offset of 1 km. The middle of the Jurassic layer, above the salt swell is highly faulted; it creates the diffractions and fault reflections visible in the middle of the section between 0.8 and 1.2 s. These reflections are affected by shallow velocity variations created by variable thickness in the low-velocity Tertiary sediments and in a high-velocity Cretaceous chalk layer; they are potential targets for showing the advantages of applying AMO prior to partial stacking. The brighter reflectors at around 1.6 s are generated at the salt-sediments interfaces. The fairly steep reflections between 1.6 and 2 s, at the left edge of the section, are caused by the flanks of the salt swells. These deeper reflections are affected not only by the shallow velocity variations, but also by the high contrast in velocity between the Jurassic and the Triassic layers.

The data-acquisition configuration was dual-source and triple streamer. The nominal common-midpoint spacing was 9.375 m in the in-line direction, and 25 m in the cross-line direction. The cable length was 2,200 m with maximum feathering of approximately 17 degrees. To make the data handling and processing quicker, we processed only a subset of the whole data set. We windowed in time the data traces up to 600 time-samples, for a maximum time of 2.4 s. We selected the central 512 midpoints in the in-line direction, for a total length of 4,800 m, and 130 midpoints in the cross-line, for a total width of 3,250 m. Figure 7 shows the offset-azimuth distribution of a small subset of the data traces. As it is typical for such acquisition geometry, the figure shows six distinct trends, which are most distinguishable at small offsets; each trend corresponding to individual source-streamer pairs.

To test the effects of AMO on the prestack data, we applied two distinct partial stacking methods to the data: NMO followed by partial stacking (NMO-stacking);

and NMO followed by AMO and partial stacking (NMO-AMO-stacking). To make the comparison as fair as possible to the conventional methodology of simple NMO-stacking, the traces after NMO were laterally interpolated in the midpoint direction before they were stacked into the output cube. Our tests showed that this lateral interpolation preserved the dipping events significantly better than a simple binning procedure.

We applied partial stacking independently on six different subsets of the data. The subsets were determined according to the absolute value of the offset. Each offset range was 400 m wide, starting from zero. The boundaries between the offset ranges are shown as vertical bars in Figure 7. For all offset ranges, the output data were a regularly sampled cube with nominal offset equal to the midpoint of the range; that is, 200, 600, 1,000, 1,400, 1,800 and 2,200 m. The number of traces input into the partial-stacking process depended on the offset range; for example, for the 800–1,200 m range the number of input traces was about 460,000. The output cube had 512 midpoints in the in-line direction, and 130 in the cross-line, for a total of 66,560 output traces. Therefore, the data-reduction achieved by partial stacking is approximately a factor of 7.

Before processing the data, we applied a hyperbolic mute with a sharp cut-off. To assure the removal of the first arrival and some severely aliased noise at the far-offset, we set the mute velocity slightly lower than water velocity. After muting, we applied NMO with a velocity function varying with midpoint and time. The NMO velocity function was given to us together with the data. No inverse NMO was applied to the results before they were plotted, thus the reflection timings are equivalent “zero-offset” times. Of course, inverse NMO must be applied before the AMO results are input into a prestack depth migration.

In general, the wider the offset and the larger the azimuth rotation, the more significant is the effect of AMO on the data. For the geometry of our data set, the most significant effects are visible for the longer offset ranges, starting from the

800 – 1,200 m range. Figure 8 compares the results obtained with the two flows described above, for the 800 – 1,200 m offset range. The figure displays a window of an in-line section, located at 19,590 m along the cross-line axis and centered on the fault blocks where the data show numerous high-frequency diffractions. Figure 8a shows the section obtained by simple NMO-stacking, while Figure 8b shows the results of NMO-AMO-stacking. As expected, the addition of AMO to the partial stacking process preserves the diffractions much better than simple NMO. Figure 8c shows the differences between the two sections; diffractions and fault reflections are clearly evident.

Figure 9 compares the time slices cut at 1.068 s, for the same offset range (800 – 1,200 m) as in Figure 8. As in Figure 8, Figure 9a shows the results of NMO-stacking, while Figure 9b shows the results of NMO-AMO-stacking. The difference section (Figure 9c) clearly shows that the high-frequency diffractions were strongly attenuated by the conventional process. The most evident differences tend to occur for reflections that are oriented at an angle with respect to the in-line direction. This observation is consistent with the fact that the conventional NMO-stacking process is most inaccurate for reflections that are oblique with respect to the nominal azimuth; the angle of maximum error is dependent on the reflector’s dip. Although there are not many such reflections in this data set, which shows geological dips mostly aligned along the in-line directions, the AMO process enhances the ones that are present.

Figure 10 compares the time slices cut at 1.1 s, for the next offset range, that is, the 1,200 – 1,600 m range. For this offset range, as in the previous one, the trend of diffractions from the fault blocks are strongly attenuated by the conventional procedure of NMO followed by partial stacking. On the contrary, AMO preserves these important events during the stacking procedure.

Figure 11 shows windows of an in-line section for the 1,200 – 1,600 m offset range. This in-line section is located at 20,940 m and centered around the salt-flank reflection visible in the lower-left corner of Figure 6. The dipping salt flank reflection is better

preserved by the application of AMO. Further, as for the shallower section, some mildly dipping reflections appear to be “cleaner” after AMO. A possible explanation for this phenomenon is that the incoherent stacking of the diffractions, and of other steeply dipping reflections, contributes to the general level of background noise in the data obtained by simple NMO-stacking.

DISCUSSIONS AND CONCLUSIONS

The AMO operator presented in this paper is a new partial prestack-migration operator that can be efficiently applied to 3-D prestack seismic data to transform their effective offset and azimuth. AMO is a generalization of the migration-to-zero-offset operators (e.g. DMO) because it can transform data to arbitrary offsets as well as azimuths.

To derive the AMO operator we analytically evaluated the operator equivalent to applying a 3-D prestack imaging operator followed by 3-D prestack modeling operator. We used DMO chained with inverse DMO, and alternatively we used constant-velocity full prestack migration chained with constant-velocity prestack modeling. The constant-velocity assumption is necessary to an analytical derivation of the AMO operator. However, because the same constant-velocity assumption is used for both the forward and the inverse operator, AMO is correct at first order even in presence of lateral velocity variations. The results of processing a marine data set demonstrate that AMO can be effectively applied to data that were acquired over complex structures and whose proper imaging requires 3-D prestack depth migration. Further testing is necessary to validate its use in even more difficult situations.

This paper showed that the application of AMO improves the accuracy of partial stacking 3-D data over a range of offsets. In particular, the high-frequency steeply-dipping components of the reflected, or diffracted, energy benefit from the application of AMO. These components are crucial for the correct interpretation of complex fault

systems, as well as for high-resolution imaging of complex reservoirs. Partial stacking is a valuable tool to reduce the cost of 3-D prestack depth migration because it reduces the size of the data to be migrated. Therefore, AMO has the potential of reducing the computational cost of 3-D prestack depth imaging, with only minimum influence on the accuracy of the results.

ACKNOWLEDGEMENTS

We would like to thank the sponsors of the Stanford Exploration Project for supporting the research presented in this paper. The project was also partially funded by the ACTI project # 4731U0015-3Q.

We would like to thank Conoco and its partners BP and Mobil, for agreeing to release the data to SEP. In particular, we would like to thank Doug Hanson of Conoco for giving us the opportunity to test our method on such an interesting data set, and for his successful efforts to actually send the data to us.

We also would like to thank the two anonymous reviewers of the paper. Their comments have been very helpful in improving the clarity and readability of the paper.

REFERENCES

- Bagaini, C., Spagnolini, U., and Paziienza, V., 1994, Velocity analysis and missing offset restoration by prestack continuation operators: 65th Ann. Internat. Meeting, Soc. Expl. Geophys., Expanded Abstracts, 1549–1552.
- Bevc, D., and Claerbout, J., 1992, Fast Anti-Aliased Kirchhoff Migration and Modeling: SEP-75, 91–96.
- Beylkin, G., 1985, Imaging of Discontinuities in the Inverse Scattering Problem by Inversion of a Causal Generalized Radon Transform: J. Math. Phys., **26**, 99–108.

- Biondi, B., and Chemingui, N., 1994, Transformation of 3-D prestack data by azimuth moveout (AMO): 65th Ann. Internat. Meeting, Soc. Expl. Geophys., Expanded Abstracts, 1541–1544.
- Biondi, B., and Palacharla, G., 1996, 3-D prestack migration of common-azimuth data: *Geophysics*, **61**, 1822–1832.
- Black, J. L., Schleicher, K., and Zhang, L., 1993, True-amplitude imaging and dip moveout: *Geophysics*, **58**, 47–66.
- Bleistein, N., and Handelsman, R. A., 1975, Asymptotic expansions of integrals: Rinehart Winston.
- Bleistein, N., 1990, Born DMO Revisited: 60th Ann. Internat. Meeting, Soc. Expl. Geophys., Expanded Abstracts, 1366–1369.
- Bolondi, G., Loinger, E., and Rocca, F., 1984, Offset continuation in theory and practice: *Geophys. Prosp.*, **32**, 1045–1073.
- Canning, A., and Gardner, G. H. F., 1996a, Regularizing 3-D data sets with DMO: *Geophysics*, **61**, 1103–1114.
- 1996b, A two-pass approximation to 3-D prestack migration: *Geophysics*, **61**, 409–421.
- Chemingui, N., and Biondi, B., 1995, Amplitude preserving azimuth moveout: 65th Ann. Internat. Meeting, Soc. Expl. Geophys., Expanded Abstracts, 1453–1456.
- Chemingui, N., and Biondi, B., 1996, Handling the irregular geometry in wide-azimuth surveys: 66th Ann. Internat. Meeting, Soc. Expl. Geophys., Expanded Abstracts, 32–35.
- Cohen, J. K., and Hagin, F. G., 1985, Velocity inversion using a stratified reference: *Geophysics*, **50**, 1689–1700.

- Deregowski, S. M., and Rocca, F., 1981, Geometrical optics and wave theory of constant offset sections in layered media: *Geophys. Prosp.*, **29**, 374–406.
- Deregowski, S. M., 1986, What is DMO: *First Break*, **4**, no. 7, 7–24.
- Fomel, S., and Biondi, B., 1995a, The time and space formulation of azimuth moveout: *SEP-84*, 25–38.
- 1995b, The time and space formulation of azimuth moveout: 65th Ann. Internat. Meeting, Soc. Expl. Geophys., Expanded Abstracts, 1449–1452.
- Goldin, S. V., 1986, Seismic travelttime inversion: SEG, Tulsa.
- Goldin, S. V., 1994, Superposition and continuation of transformations used in seismic migration: *Russian Geology and Geophysics*, **35**, no. 9, 109–121.
- Gray, S. H., 1992, Frequency-selective design of the Kirchhoff migration operator: *Geophys. Prosp.*, **40**, 565–571.
- Hale, D., 1984, Dip-moveout by Fourier transform: *Geophysics*, **49**, 741–757.
- Hale, D., 1991, A nonaliased integral method for dip moveout: *Geophysics*, **56**, 795–805.
- Hanson, D. W., and Witney, S. A., 1995, 3-D prestack depth migration – velocity model building and case history: 1995 Spring Symposium of the Geophys. Soc. of Tulsa, Soc. Expl. Geophys., *Seismic Depth Estimation*, 27–52.
- Hubral, P., Schleicher, J., and Tygel, M., 1996, A unified approach to 3-D seismic reflection imaging, Part I: Basic concepts: *Geophysics*, **61**, 742–758.
- Liner, C. L., and Cohen, J. K., 1988, An amplitude-preserving inverse of Hale’s DMO: 58th Ann. Internat. Meeting, Soc. Expl. Geophys., Expanded Abstracts, 117–1120.

- Liner, C. L., 1990, General theory and comparative anatomy of dip moveout: *Geophysics*, **55**, 595–607.
- Lumley, D. E., Claerbout, J. F., and Bevc, D., 1994, Anti-aliased Kirchhoff 3-D migration: Anti-aliased Kirchhoff 3-D migration:, 64th Ann. Internat. Meeting, Soc. Expl. Geophys., Expanded Abstracts, 1282–1285.
- Ronen, J., 1987, Wave-equation trace interpolation: *Geophysics*, **52**, 973–984.
- Stovas, A. M., and Fomel, S. B., 1996, Kinematically equivalent integral DMO operators: *Russian Geology and Geophysics*, **37**, no. 2, 102–113.
- Zhang, L., 1988, A new Jacobian for dip moveout: *SEP*–**59**, 201–208.
- Zhou, C., and Schuster, G. T., 1995, Quasi-random migration of 3-D field data: 65th Ann. Internat. Meeting, Soc. Expl. Geophys., Expanded Abstracts, 1145–1148.

**APPENDIX A—AMO AS A CHAIN OF DMO AND INVERSE DMO:
FREQUENCY-WAVENUMBER DOMAIN DERIVATION**

The derivation of the AMO operator starts from the Fourier-domain formulation of DMO (Hale, 1984) and “inverse” DMO (Ronen, 1987; Liner, 1990). However, because 3-D prestack data is often irregularly sampled, AMO is most conveniently applied as an integral operator in the time-space domain. To derive a time-space representation of the AMO impulse response from its frequency-wavenumber representation, we evaluate the stationary-phase approximation of the inverse Fourier transform along the midpoint coordinates.

The DMO operator and its inverse (DMO^{-1}) can be defined in the zero-offset frequency ω_0 and the midpoint wavenumber \mathbf{k} as

$$\text{DMO} = \int dt_1 J_1 e^{-i\omega_0 t_1} \sqrt{1 + \left(\frac{\mathbf{k} \cdot \mathbf{h}_1}{\omega_0 t_1}\right)^2} \quad (\text{A-1})$$

$$\text{DMO}^{-1} = \int d\omega_0 J_2 e^{+i\omega_0 t_2} \sqrt{1 + \left(\frac{\mathbf{k} \cdot \mathbf{h}_2}{\omega_0 t_2}\right)^2}. \quad (\text{A-2})$$

The AMO operator is given by the chaining of DMO and DMO^{-1} ; its impulse response can be written as,

$$\text{AMO} = \frac{1}{4\pi^2} \int d\mathbf{k} e^{-i\mathbf{k} \cdot \mathbf{m}} \int dt_1 \int d\omega_0 J_1 J_2 e^{-i\omega_0 \left(t_1 \sqrt{1 + \left(\frac{\mathbf{k} \cdot \mathbf{h}_1}{\omega_0 t_1}\right)^2} - t_2 \sqrt{1 + \left(\frac{\mathbf{k} \cdot \mathbf{h}_2}{\omega_0 t_2}\right)^2} \right)}. \quad (\text{A-3})$$

The derivation of the stationary-phase approximation of the integral in $d\mathbf{k}$ is fairly lengthy and complex. The following outline has a similar flavor to the stationary-phase approximation of the conventional DMO impulse response presented in (Black et al., 1993). We begin by changing the order of the integrals and rewriting (A-3) as

$$\text{AMO} = \frac{1}{4\pi^2} \int dt_1 \int d\omega_0 \int d\mathbf{k} J_1 J_2 e^{i[\omega_0(t_1 \eta_1 - t_2 \eta_2) - \mathbf{k} \cdot \mathbf{\Delta m}]}. \quad (\text{A-4})$$

The phase of this integral is,

$$\Phi \equiv \omega_o(t_1\eta_1 - t_2\eta_2) - \mathbf{k} \cdot \Delta\mathbf{m}, \quad (\text{A-5})$$

where,

$$\eta_1 = \sqrt{1 + \left(\frac{\mathbf{k} \cdot \mathbf{h}_1}{\omega_o t_1}\right)^2} \quad \text{and} \quad \eta_2 = \sqrt{1 + \left(\frac{\mathbf{k} \cdot \mathbf{h}_2}{\omega_o t_2}\right)^2}. \quad (\text{A-6})$$

Next we let

$$\beta_1 = \frac{\mathbf{h}_1 \cdot \mathbf{k}}{\omega_o t_1} \quad \text{and} \quad \beta_2 = \frac{\mathbf{h}_2 \cdot \mathbf{k}}{\omega_o t_2}. \quad (\text{A-7})$$

Therefore, η_1 and η_2 become

$$\eta_1 = \sqrt{1 + \beta_1^2} \quad \text{and} \quad \eta_2 = \sqrt{1 + \beta_2^2}. \quad (\text{A-8})$$

The derivatives of η_1 and η_2 with respect to the in-line component of the wavenumber k_x and the cross-line component k_y can be written as

$$\begin{aligned} \frac{\partial \eta_1}{\partial k_x} &= \frac{h_{1x}}{\omega_o t_1} \frac{\beta_1}{\sqrt{1 + \beta_1^2}} & \text{and} & \quad \frac{\partial \eta_2}{\partial k_x} = \frac{h_{2x}}{\omega_o t_1} \frac{\beta_2}{\sqrt{1 + \beta_2^2}} \\ \frac{\partial \eta_1}{\partial k_y} &= \frac{h_{1y}}{\omega_o t_1} \frac{\beta_1}{\sqrt{1 + \beta_1^2}} & \text{and} & \quad \frac{\partial \eta_2}{\partial k_y} = \frac{h_{2y}}{\omega_o t_1} \frac{\beta_2}{\sqrt{1 + \beta_2^2}}. \end{aligned} \quad (\text{A-9})$$

Making one more change of variables, we let

$$\nu_1 = \frac{\beta_1}{\sqrt{1 + \beta_1^2}} \quad \text{and} \quad \nu_2 = \frac{\beta_2}{\sqrt{1 + \beta_2^2}}. \quad (\text{A-10})$$

Setting the derivative of the phase Φ to zero yields the system of equations:

$$\begin{cases} h_{1x}\nu_1 - h_{2x}\nu_2 = \Delta m_x \\ h_{1y}\nu_1 - h_{2y}\nu_2 = \Delta m_y \end{cases} \quad (\text{A-11})$$

which we solve for ν_1 and ν_2 (i.e., η_1 and η_2) at the stationary path \mathbf{k}_0 . The determinant of the system is given by

$$\Delta = h_{2x}h_{1y} - h_{1x}h_{2y} = h_1 h_2 \sin \Delta\theta, \quad (\text{A-12})$$

and the solutions for ν_1 and ν_2 are

$$\nu_{01} = \frac{\Delta m \sin(\theta_2 - \Delta\varphi)}{h_1 \sin \Delta\theta}, \quad (\text{A-13})$$

and

$$\nu_{02} = \frac{\Delta m \sin(\theta_1 - \Delta\varphi)}{h_2 \sin \Delta\theta}. \quad (\text{A-14})$$

Now we need to evaluate the phase function Φ along the stationary path \mathbf{k}_0 . By respectively multiplying the equations in (A-11) by k_{0x} and k_{0y} and summing them we obtain,

$$\mathbf{k}_0 \cdot \Delta\mathbf{m} = \frac{\omega_o t_1 \beta_{01}^2}{\sqrt{1 + \beta_{01}^2}} - \frac{\omega_o t_2 \beta_{02}^2}{\sqrt{1 + \beta_{02}^2}}. \quad (\text{A-15})$$

Substituting (A-15) into the expression for the phase function [equation (A-5)] we obtain

$$\Phi_0 = \omega_o \left(\frac{t_1}{\sqrt{1 + \beta_{01}^2}} - \frac{t_2}{\sqrt{1 + \beta_{02}^2}} \right) = \omega_o \left(\frac{t_1}{\eta_{01}} - \frac{t_2}{\eta_{02}} \right). \quad (\text{A-16})$$

The phase function along the stationary path is thus peaked for

$$t_2 = t_1 \frac{\eta_{02}}{\eta_{01}} = t_1 \frac{\sqrt{1 - \nu_{01}^2}}{\sqrt{1 - \nu_{02}^2}}. \quad (\text{A-17})$$

Substituting equations (A-13) and (A-14) into (A-17) we obtain (1) of the main text:

$$t_2 = t_1 \frac{h_2}{h_1} \sqrt{\frac{h_1^2 \sin^2 \Delta\theta - \Delta m^2 \sin^2(\theta_2 - \Delta\varphi)}{h_2^2 \sin^2 \Delta\theta - \Delta m^2 \sin^2(\theta_1 - \Delta\varphi)}}. \quad (\text{A-18})$$

Next we derive an expression for the amplitudes of the AMO impulse response. The general expression for the stationary-phase approximation of the \mathbf{k} integral in equation (A-3) is (Bleistein and Handelsman, 1975),

$$A \approx \frac{2\pi J_1 J_2}{|\det(\mathfrak{C})|^{1/2}} e^{i\Phi + \text{sig}(\mathfrak{C}) \frac{\pi}{4}}. \quad (\text{A-19})$$

Therefore we need to evaluate the determinant and the signature of the curvature matrix \mathfrak{C} , which is defined as

$$\mathfrak{C} = \begin{vmatrix} \frac{\partial^2 \Phi}{\partial k_x^2} & \frac{\partial^2 \Phi}{\partial k_x \partial k_y} \\ \frac{\partial^2 \Phi}{\partial k_x \partial k_y} & \frac{\partial^2 \Phi}{\partial k_y^2} \end{vmatrix}. \quad (\text{A-20})$$

Taking the second-order partial derivatives of Φ with respect to k_x and k_y and using the definitions of β_1 and β_2 yields the following expressions for $\frac{\partial^2 \Phi}{\partial k_x^2}$, $\frac{\partial^2 \Phi}{\partial k_y^2}$ and $\frac{\partial^2 \Phi}{\partial k_x \partial k_y}$:

$$\frac{\partial^2 \Phi}{\partial k_x^2} = \frac{h_{1x}^2}{w_o t_1} (1 - \nu_{01}^2)^{3/2} - \frac{h_{2x}^2}{\omega_o t_2} (1 - \nu_{02}^2)^{3/2}, \quad (\text{A-21})$$

$$\frac{\partial^2 \Phi}{\partial k_y^2} = \frac{h_{1y}^2}{w_o t_1} (1 - \nu_{01}^2)^{3/2} - \frac{h_{2y}^2}{\omega_o t_2} (1 - \nu_{02}^2)^{3/2}, \quad (\text{A-22})$$

and

$$\frac{\partial^2 \Phi}{\partial k_x \partial k_y} = \frac{h_{1x} h_{1y}}{w_o t_1} (1 - \nu_{01}^2)^{3/2} - \frac{h_{2x} h_{2y}}{\omega_o t_2} (1 - \nu_{02}^2)^{3/2}. \quad (\text{A-23})$$

With a little algebra, one may verify that the determinant of the curvature matrix is

$$\begin{aligned} \det(C) &= -\frac{\Delta^2}{|\omega_o|^2 t_1 t_2} (1 - \nu_{01}^2)^{3/2} (1 - \nu_{02}^2)^{3/2} \\ &= -\frac{\Delta^2}{|\omega_o|^2 t_0^2} (1 - \nu_{01}^2)^2 (1 - \nu_{02}^2)^2. \end{aligned} \quad (\text{A-24})$$

We notice that the determinant of \mathfrak{C} , which is the product of the two eigenvalues of \mathfrak{C} , is always negative; that is, that the two eigenvalues have opposite signs and thus the signature of \mathfrak{C} , which is defined as the number of positive eigenvalues minus the number of negative eigenvalues, is always null. Therefore, the second term of the phase shift in equation (A-19) vanishes.

To obtain expressions for the AMO amplitude, we need to substitute equation (A-24) into equation (A-19), together with the corresponding expressions for J_1 and J_2 . For the Jacobian J_1 of the forward DMO we can use any of the Jacobians proposed in the literature by Hale (1984), Zhang and Black (1988), and Bleistein (1990). The Jacobian J_2 of inverse DMO can be derived with Beylkin's theory for the asymptotic inverse of stacking operators (Beylkin, 1985; Cohen and Hagin, 1985). The expression for the Jacobian of the asymptotic inverse for Hale's DMO were derived by Liner and

Cohen (1988). Chemingui and Biondi (1995) and Fowler (personal communication) independently derived the inverse for Zhang-Black's DMO. As mentioned in the main text, we used Zhang-Black's Jacobians for the actual application of AMO; that is,

$$J_1 = \frac{(1 + \nu_{01}^2)}{\sqrt{1 - \nu_{01}^2}}, \quad J_2 = 1. \quad (\text{A-25})$$

Finally, after taking into account the Jacobian of the transformation from t_1 to t_0 ($dt_1 = dt_0\sqrt{1 - \nu_{01}^2}$) in the first integral of equation (A-4), we can write the amplitude term for the AMO integral:

$$A \approx \frac{|\omega_o| t_0}{2\pi\Delta} \frac{(1 + \nu_{01}^2)}{(1 - \nu_{01}^2)(1 - \nu_{02}^2)} \quad (\text{A-26})$$

$$= \frac{|\omega_2| t_2}{2\pi\Delta} \frac{(1 + \nu_{01}^2)}{(1 - \nu_{01}^2)(1 - \nu_{02}^2)}. \quad (\text{A-27})$$

The last substitution, $|\omega_o| t_0 = |\omega_2| t_2$, enables us to apply the differentiation operator $|\omega_2|$ to the output data; this is correct because t_0 and t_2 are linked by the linear relationship $t_0 = t_2\sqrt{1 - \nu_{02}^2}$.

The expression for the amplitudes presented in equation (5) of the main text follows by substitution of the expressions for Δ , ν_{01} , and ν_{02} , from equations (A-12), (A-13) and (A-14) into equation (A-27).

2-D AMO operator

When the input offset h_1 is parallel to the output offset h_2 , the determinant [equation (A-12)] of the system (A-11) is equal to zero. In this case, as we discussed in the main text, the 3-D AMO operator degenerates into a 2-D operator. The fact that the determinant of the system of equations is equal to zero means that the two equations are linearly dependent, and that we are left with only one equation. However, because the operator is two-dimensional, the number of components of the unknown \mathbf{k}_0 also goes from two to one. Consequently, another stationary-phase approximation to the AMO operator can be found. The new equation is a quartic,

and unfortunately, we have not been able to solve this new equation analytically. However, we have found the solution for the kinematics of the operator with the help of Mathematica; the resulting expression for the 2-D AMO operator is presented in equation (4) of the main text.

**APPENDIX B—AMO AS A CHAIN OF DMO AND INVERSE DMO:
TIME-SPACE DOMAIN DERIVATION**

In this appendix, we present an alternative derivation of the AMO operator. The entire derivation is carried out in the time-space domain. It applies the idea of chaining DMO and inverse DMO, developed in appendix A, but uses the integral formulation of DMO (Deregowski and Rocca, 1981; Deregowski, 1986; Hale, 1991) in place of the frequency-domain DMO.

Let $P_1(\mathbf{m}_1, t_1; \mathbf{h}_1)$ be the input of an AMO operator (common-azimuth and common-offset seismic reflection data after normal moveout correction) and $P_2(\mathbf{m}_2, t_2; \mathbf{h}_2)$ be the output. Then the three-dimensional AMO operator takes the following general form:

$$P_2(\mathbf{m}_2, t_2; \mathbf{h}_2) = |\mathbf{D}_{t_2}| \int \int w_{12}(\Delta \mathbf{m}, \mathbf{h}_1, \mathbf{h}_2, t_2) P_1(\mathbf{m}_1, t_2 \sigma_{12}(\Delta \mathbf{m}, \mathbf{h}_1, \mathbf{h}_2); \mathbf{h}_1) d\mathbf{m}_1, \quad (\text{B-1})$$

where $|\mathbf{D}_{t_2}|$ is the differentiation operator (equivalent to multiplication by $|\omega_2|$ in the frequency domain), $\Delta \mathbf{m} = \mathbf{m}_2 - \mathbf{m}_1$ is the difference vector between the input and the output midpoints, $t_2 \sigma_{12}$ is the summation path, and w_{12} is the weighting function.

To derive (B-1) in the time-space domain we chain an integral DMO operator of the form

$$P_0(\mathbf{m}_0, t_0; \mathbf{0}) = \mathbf{D}_{-t_0}^{1/2} \int w_{10}(\Delta \mathbf{m}_{10}, \mathbf{h}_1, t_0) P_1(\mathbf{m}_1, t_0 \sigma_{10}(\Delta \mathbf{m}_{10}, \mathbf{h}_1); \mathbf{h}_1) d\hat{x}_1 \quad (\text{B-2})$$

with an inverse DMO of the form

$$P_2(\mathbf{m}_2, t_2; \mathbf{h}_2) = \mathbf{D}_{t_2}^{1/2} \int w_{02}(\Delta \mathbf{m}_{02}, \mathbf{h}_2, t_2) P_0(\mathbf{m}_0, t_2 \sigma_{02}(\Delta \mathbf{m}_{02}, \mathbf{h}_2); \mathbf{0}) d\hat{x}_0. \quad (\text{B-3})$$

Where $t_0 \sigma_{10}$ and $t_2 \sigma_{02}$ are the summation paths of the DMO and inverse DMO operators (Deregowski and Rocca, 1981):

$$\sigma_{10}(\Delta \mathbf{m}, \mathbf{h}_1) = \frac{h_1}{\sqrt{h_1^2 - \Delta m^2}}, \quad \sigma_{02}(\Delta \mathbf{m}, \mathbf{h}_2) = \frac{\sqrt{h_2^2 - \Delta m^2}}{h_2}; \quad (\text{B-4})$$

w_{10} and w_{02} are the corresponding weighting functions (amplitudes of impulse responses); \hat{x}_1 is the component of \mathbf{m}_1 along the \mathbf{h}_1 azimuth; \hat{x}_0 is the component of \mathbf{m}_0 along the \mathbf{h}_2 azimuth; and $\Delta\mathbf{m}_{10} = \mathbf{m}_0 - \mathbf{m}_1$, $\Delta\mathbf{m}_{02} = \mathbf{m}_2 - \mathbf{m}_0$. $\mathbf{D}_t^{1/2}$ stands for the operator of half-order differentiation (equivalent to the multiplication by $(i\omega)^{1/2}$ in the Fourier domain).

Both DMO and inverse DMO operate as 2-D operators on 3-D seismic data, because their apertures are defined on a line. This implies that for a given input midpoint \mathbf{m}_1 , the corresponding location of \mathbf{m}_0 must belong to the line going through \mathbf{m}_1 , with the azimuth θ_1 defined by the input offset \mathbf{h}_1 . Similarly, \mathbf{m}_0 must be on the line going through \mathbf{m}_2 with the azimuth θ_2 of \mathbf{h}_2 . These geometrical considerations lead us to the following conclusion: *For a given pair of input and output midpoints \mathbf{m}_1 and \mathbf{m}_2 of the AMO operator, the corresponding midpoint \mathbf{m}_0 on the intermediate zero-offset gather is determined by the intersection of two lines drawn through \mathbf{m}_1 and \mathbf{m}_2 in the offset directions.* Applying the geometric connection among the three midpoints, we can find the chain of the DMO and inverse DMO operators in one step. For this purpose, it is sufficient to notice that the angles in the triangle, formed by the midpoints \mathbf{m}_1 , \mathbf{m}_0 , and \mathbf{m}_2 , satisfy the law of sines:

$$\left| \frac{\Delta m}{\sin \Delta\theta} \right| = \left| \frac{\Delta m_{10}}{\sin(\theta_2 - \Delta\varphi)} \right| = \left| \frac{\Delta m_{02}}{\sin(\theta_1 - \Delta\varphi)} \right|. \quad (\text{B-5})$$

Substituting equation (B-2) into (B-3), taking into account (B-5), and neglecting the low-order asymptotic terms, produces the 3-D integral AMO operator (B-1), where

$$\begin{aligned} \sigma_{12}(\Delta\mathbf{m}, \mathbf{h}_1, \mathbf{h}_2) &= \sigma_{02}(\Delta\mathbf{m}_{02}, \mathbf{h}_2) \sigma_{10}(\Delta\mathbf{m}_{10}, \mathbf{h}_1) \\ &= \frac{h_1}{h_2} \sqrt{\frac{h_2^2 - \Delta m_{02}^2}{h_1^2 - \Delta m_{10}^2}} \\ &= \frac{h_1}{h_2} \sqrt{\frac{h_2^2 \sin^2 \Delta\theta - \Delta m^2 \sin^2(\theta_1 - \Delta\varphi)}{h_1^2 \sin^2 \Delta\theta - \Delta m^2 \sin^2(\theta_2 - \Delta\varphi)}}, \end{aligned} \quad (\text{B-6})$$

and

$$w_{12}(\Delta \mathbf{m}, \mathbf{h}_1, \mathbf{h}_2, t_2) = \frac{w_{02}(\Delta \mathbf{m}_{02}, \mathbf{h}_2, t_2) w_{10}[\Delta \mathbf{m}_{10}, \mathbf{h}_1, t_2 \sigma_{02}(\Delta \mathbf{m}_{02}, \mathbf{h}_2)]}{\sin \Delta \theta}. \quad (\text{B-7})$$

Equation (B-6) is the reciprocal of, and thus equivalent to equation (1) in the main text. The factor $\sin \Delta \theta$ in the denominator of the equation (B-7) appears as the result of the midpoint-coordinate transformation $d\mathbf{m}_1 = d\hat{x}_0 d\hat{x}_1 \sin \Delta \theta$.

The time-and-space analogue of amplitude-preserving DMO (Black et al., 1993) has the weighting function

$$w_{10}(\Delta \mathbf{m}_{10}, \mathbf{h}_1, t_0) = \sqrt{\frac{t_0}{2\pi}} \frac{h_1^2 + \Delta m_{10}^2}{h_1 (h_1^2 - \Delta m_{10}^2)} \quad (\text{B-8})$$

while its asymptotic inverse has the weighting function

$$w_{02}(\Delta \mathbf{m}_{02}, \mathbf{h}_2, t_2) = \sqrt{\frac{t_2}{2\pi}} \frac{h_2}{(h_2^2 - \Delta m_{02}^2)}. \quad (\text{B-9})$$

Inserting (B-8) and (B-9) into (B-7), and using the equality $\sqrt{\mathbf{D}_{-t_2} t_2} = \sqrt{\mathbf{D}_{-t_0} t_0}$, similarly to appendix A, yields

$$w_{12}(\Delta \mathbf{m}, \mathbf{h}_1, \mathbf{h}_2, t_2) = \frac{t_2}{2\pi h_1 h_2 \sin \Delta \theta} \frac{1 + \frac{\Delta m^2 \sin^2(\theta_2 - \Delta \varphi)}{h_1^2 \sin^2 \Delta \theta}}{\left(1 - \frac{\Delta m^2 \sin^2(\theta_2 - \Delta \varphi)}{h_1^2 \sin^2 \Delta \theta}\right) \left(1 - \frac{\Delta m^2 \sin^2(\theta_1 - \Delta \varphi)}{h_2^2 \sin^2 \Delta \theta}\right)}, \quad (\text{B-10})$$

which is equivalent to equation (5) in the main text.

2-D AMO operator

When the input-offset vector \mathbf{h}_1 is parallel to the output-offset vector \mathbf{h}_2 , the triangle $\mathbf{m}_1\text{-}\mathbf{m}_0\text{-}\mathbf{m}_2$, formed by the midpoints of the input trace, zero-offset trace, and output trace, degenerates to a line. The location of the zero-offset midpoint \mathbf{m}_0 is not constrained by the input and output midpoints and can take different values on the line. The chain of DMO and inverse DMO becomes a convolution on that line. To find the summation path of 2-D AMO (offset continuation), one needs to consider the envelope of the family of traveltime curves, where m_0 is the parameter of a curve in the family:

$$t_1 = t_2 \sigma_{12}(m_1, m_2, h_1, h_2) = t_2 \left| \frac{h_1}{h_2} \right| \sqrt{\frac{h_2^2 - (m_2 - m_0)^2}{h_1^2 - (m_1 - m_0)^2}}. \quad (\text{B-11})$$

Solving the envelope condition $\frac{\partial \sigma_{12}}{\partial m_0} = 0$ for the zero-offset midpoint m_0 produces

$$m_0 = \frac{(\Delta m)^2 + h_2^2 - h_1^2 + \text{sign}(h_1^2 - h_2^2) \sqrt{((\Delta m)^2 - h_1^2 - h_2^2)^2 - 4 h_1^2 h_2^2}}{2 (\Delta m)}, \quad (\text{B-12})$$

where $\Delta m = m_1 - m_2$. Substituting (B-12) into (B-11), we obtain the explicit expression (4) for the offset continuation summation path.

APPENDIX C—AMO APERTURE: CHAINING MIGRATION AND MODELING

Chaining DMO and inverse DMO allowed the analytical evaluation of the AMO operator’s summation path and the corresponding weighting function. However, this procedure is not sufficient for evaluating the third major component of the integral operator; that is, its aperture (range of integration). To solve this problem, we define AMO as the chain of the 3-D common-offset common-azimuth migration and the 3-D modeling for a different azimuth and offset.

The impulse response of common-offset common-azimuth migration is a symmetric ellipsoid with the center in the input midpoint and axis of symmetry along the input-offset direction. Such an ellipsoid is described by the general formula

$$z(\mathbf{m}) = \sqrt{R^2 - \Delta m^2 + \gamma \frac{(\Delta \mathbf{m} \cdot \mathbf{h}_1)^2}{h_1^2}}, \quad (\text{C-1})$$

where z is the depth coordinate, \mathbf{m} is the surface coordinate, $\Delta \mathbf{m} = \mathbf{m} - \mathbf{m}_1$, R is the small semi-axis of the ellipsoid, and γ is a nondimensional parameter describing the stretching of the ellipse ($\gamma < 1$). Deregowski and Rocca (1981) derived the following connections

$$R = \frac{v t_1}{2} \text{ and } \gamma = \frac{\frac{4h_1^2}{v^2}}{t_1^2 + \frac{4h_1^2}{v^2}}, \quad (\text{C-2})$$

between the geometric properties of the reflector and the coordinates of the corresponding impulse in the data: where v is the propagation velocity.

The impulse response of the AMO operator corresponds kinematically to the reflections from the ellipsoid defined by equation (C-1) to a different azimuth and different offset. To constrain the AMO aperture, we should look for the answer to the following question: *For a given elliptic reflector defined by the input midpoint, offset, and time coordinates, what points on the surface can form a source-receiver pair valid for a reflection?* If a point in the output midpoint-offset space cannot be related to a reflection pattern, it should be excluded from the AMO aperture.

Fermat's principle provides a general method of solving the kinematic reflection problem (Goldin, 1986). The formal expression for the two-point reflection traveltime is given by

$$t_2 = \frac{\sqrt{(\mathbf{s}_2 - \mathbf{m})^2 + z^2(\mathbf{m})}}{v} + \frac{\sqrt{(\mathbf{r}_2 - \mathbf{m})^2 + z^2(\mathbf{m})}}{v}, \quad (\text{C-3})$$

where \mathbf{m} is the vertical projection of the reflection point to the surface, \mathbf{s}_2 is the source location, and \mathbf{r}_2 is the receiver location for the output trace. According to Fermat's principle, the reflection raypath between two fixed points must correspond to the extremum value of the traveltime. Hence, in the vicinity of a reflected ray,

$$\frac{\partial t_2}{\partial \mathbf{m}} = 0. \quad (\text{C-4})$$

Solving equation (C-4) for \mathbf{m} allows us to find the reflection raypath for a given source-receiver pair on the surface.

To find the solution of (C-4), it is convenient to decompose the reflection-point projection \mathbf{m} into three components: $\mathbf{m} = \mathbf{m}_1 + \mathbf{m}_{\parallel} + \mathbf{m}_{\perp}$, where \mathbf{m}_{\parallel} is parallel to the input offset vector \mathbf{h}_1 , and \mathbf{m}_{\perp} is perpendicular to \mathbf{h}_1 . The plane, drawn through the reflection point and the central line of ellipsoid (C-1), must contain the zero-offset (normally reflected) ray because of the cylindrical symmetry of the reflector. The fact that the zero-offset ray is normal to the reflector gives us the following connection

$$\mathbf{m}_0 = (\mathbf{m}_1 + \mathbf{m}_{\parallel}) + z \left(\mathbf{m}_1 + \mathbf{m}_{\parallel} \right) \frac{\partial z}{\partial (\mathbf{m}_1 + \mathbf{m}_{\parallel})} = \mathbf{m}_1 + \gamma \mathbf{m}_{\parallel}, \quad (\text{C-5})$$

between the zero-offset midpoint \mathbf{m}_0 and the \mathbf{m}_{\parallel} component of the reflection point \mathbf{m} . Equation (C-5) evaluates \mathbf{m}_{\parallel} in terms of \mathbf{m}_0 , as follows:

$$\mathbf{m}_{\parallel} = \frac{\Delta \mathbf{m}_{10}}{\gamma}. \quad (\text{C-6})$$

where the length of the vector $\Delta \mathbf{m}_{10} = \mathbf{m}_0 - \mathbf{m}_1$ can be determined from equation (B-5) for any given input and output midpoints \mathbf{m}_1 and \mathbf{m}_2 and azimuths θ_1 and θ_2 .

To find the third component of the reflection point projection (\mathbf{m}_{\perp}), we substitute expression (C-6) into (C-3). Choosing a convenient parameterization $\mathbf{s}_2 = \mathbf{m}_0 + \mathbf{h}_2^s$,

$\mathbf{r}_2 = \mathbf{m}_0 + \mathbf{h}_2^r$, where $\mathbf{h}_2^r - \mathbf{h}_2^s = 2 \mathbf{h}_2$, and $\mathbf{h}_2^r + \mathbf{h}_2^s = 2 \Delta \mathbf{m}_{02} = 2 (\mathbf{m}_2 - \mathbf{m}_0)$, we can rewrite the two-point traveltime function from (C-3) in the form

$$t_2 = \frac{\sqrt{R^2 - \gamma(1-\gamma)m_{\parallel}^2 + (h_2^s)^2 - 2 \mathbf{h}_2^s \cdot (\mathbf{m}_{\perp} + (1-\gamma) \mathbf{m}_{\parallel})}}{v} + \frac{\sqrt{R^2 - \gamma(1-\gamma)m_{\parallel}^2 + (h_2^r)^2 - 2 \mathbf{h}_2^r \cdot (\mathbf{m}_{\perp} + (1-\gamma) \mathbf{m}_{\parallel})}}{v}. \quad (\text{C-7})$$

Fermat's principle (C-4) leads to a simple linear equation for the length of \mathbf{m}_{\perp} , which has the explicit solution

$$m_{\perp} = (\gamma - 1) m_{\parallel} \cot(\theta_2 - \theta_1) - \frac{h_2 (R^2 - \gamma(1-\gamma)m_{\parallel}^2)}{(h_2^2 - (\Delta m_{02})^2) \sin(\theta_2 - \theta_1)}, \quad (\text{C-8})$$

where m_{\parallel} is defined by (C-6), and Δm_{02} satisfies relationship (B-5).

Because the reflection point is contained inside the ellipsoid, its projection obeys the inequality

$$z^2(\mathbf{m}) = R^2 - m_{\perp}^2 - (1-\gamma)m_{\parallel}^2 \geq 0, \quad (\text{C-9})$$

that defines the aperture of the AMO operator. After transformation (6) and algebraic simplifications, it takes the form of inequality (13), which is convenient for an efficient implementation of AMO.

FIGURES

FIG. 1. The full AMO impulse response ($V_{min} \simeq 0$) when $t_1 = 1$ s, $h_1 = 2$ km, $h_2 = 1.8$ km, $\theta_1 = 0^\circ$, $\theta_2 = 30^\circ$.

FIG. 2. The maximum spatial support of the AMO operator (shaded parallelogram) in the midpoint plane ($\Delta m_x, \Delta m_y$), as a function of the input offset \mathbf{h}_1 , and the output offset \mathbf{h}_2 .

FIG. 3. The effective AMO impulse response when $V_{min} = 2$ km/s, and $t_1 = 1$ s, $h_1 = 2$ km, $h_2 = 1.8$ km, $\theta_1 = 0^\circ$, $\theta_2 = 30^\circ$. Compare with Figure 1.

FIG. 4. The geometric relationship between the unit vectors ξ_1 and ξ_2 of the transformed midpoint-coordinate axes, and the input offset \mathbf{h}_1 and the output offset \mathbf{h}_2 .

FIG. 5. Geological in-line section and corresponding velocities of layers. From (Hanson and Witney, 1995).

FIG. 6. In-line section of the North Sea data set used for testing AMO.

FIG. 7. Offset-azimuth distribution of the test data set. The vertical bars show the boundaries among the offset ranges that were used for partial stacking.

FIG. 8. In-line sections (19,590 m) for the 800 – 1,200 m offset range, obtained by a) NMO-stacking, b) NMO-AMO-stacking, c) subtracting a) from b).

FIG. 9. Time slices (1.068 s) for the 800 – 1,200 m offset range, obtained by a) NMO-stacking, b) NMO-AMO-stacking, c) subtracting a) from b).

FIG. 10. Time slices (1.068 s) for the 1,200 – 1,600 m offset range, obtained by a) NMO-stacking, b) NMO-AMO-stacking, c) subtracting a) from b).

FIG. 11. In-line sections (20,940 m) for the 1,200 – 1,600 m offset range, obtained by a) NMO-stacking, b) NMO-AMO-stacking, c) subtracting a) from b).

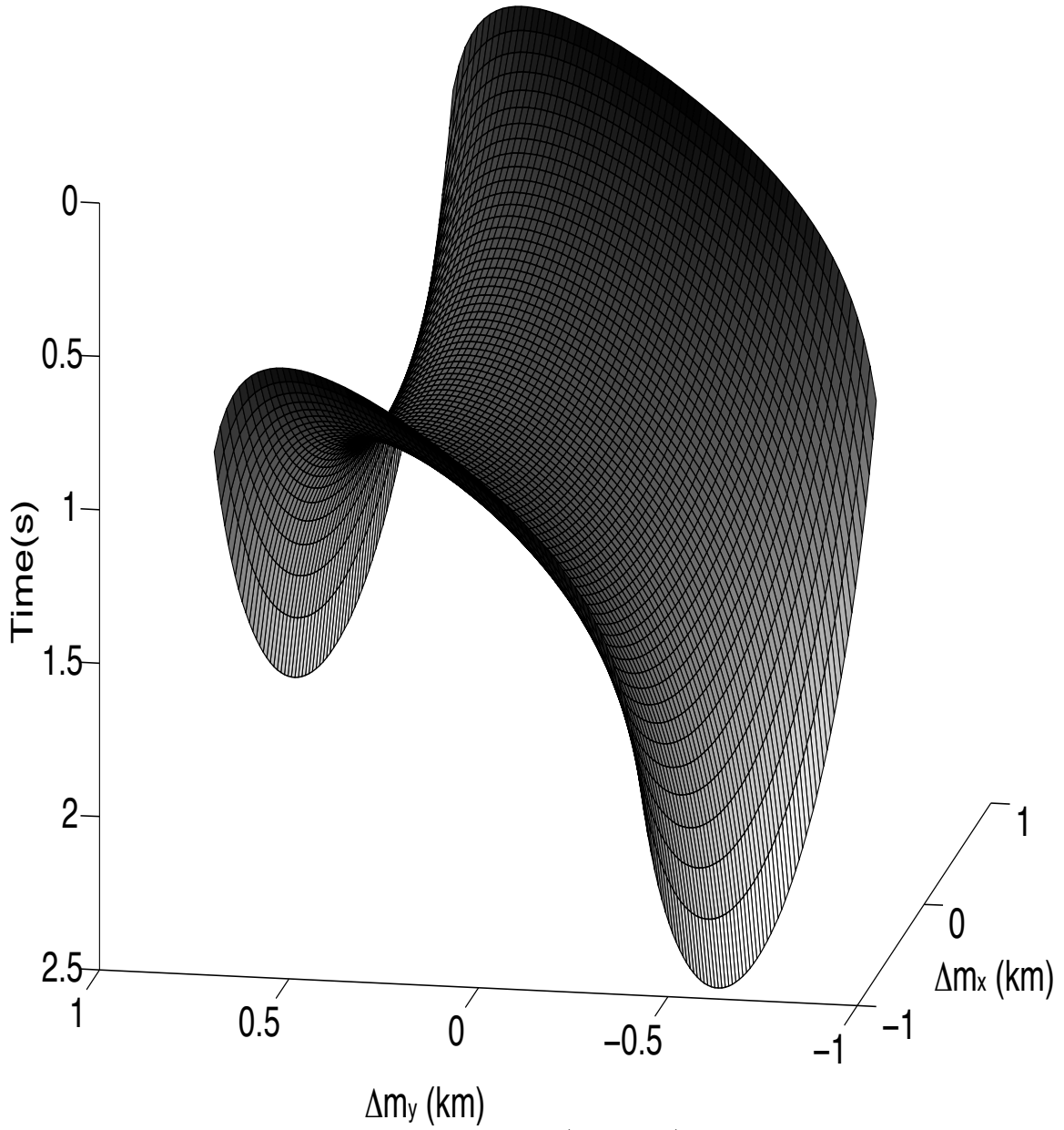


FIG. 1. The full AMO impulse response ($V_{min} \simeq 0$) when $t_1 = 1$ s, $h_1 = 2$ km, $h_2 = 1.8$ km, $\theta_1 = 0^\circ$, $\theta_2 = 30^\circ$.

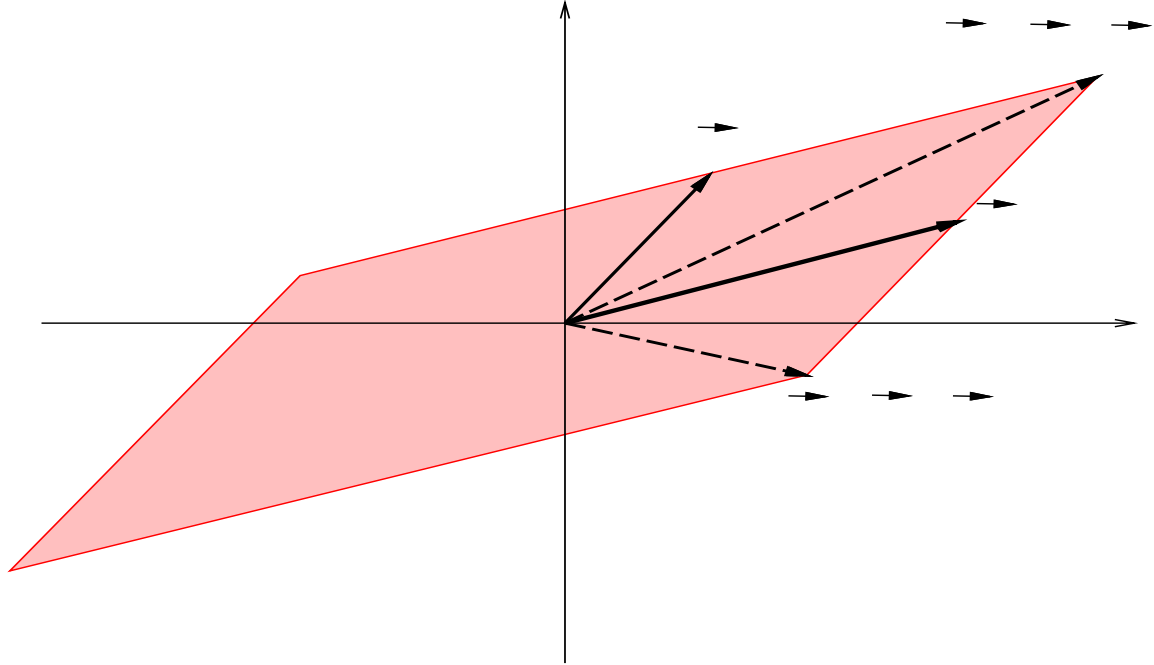


FIG. 2. The maximum spatial support of the AMO operator (shaded parallelogram) in the midpoint plane $(\Delta m_x, \Delta m_y)$, as a function of the input offset \mathbf{h}_1 , and the output offset \mathbf{h}_2 .

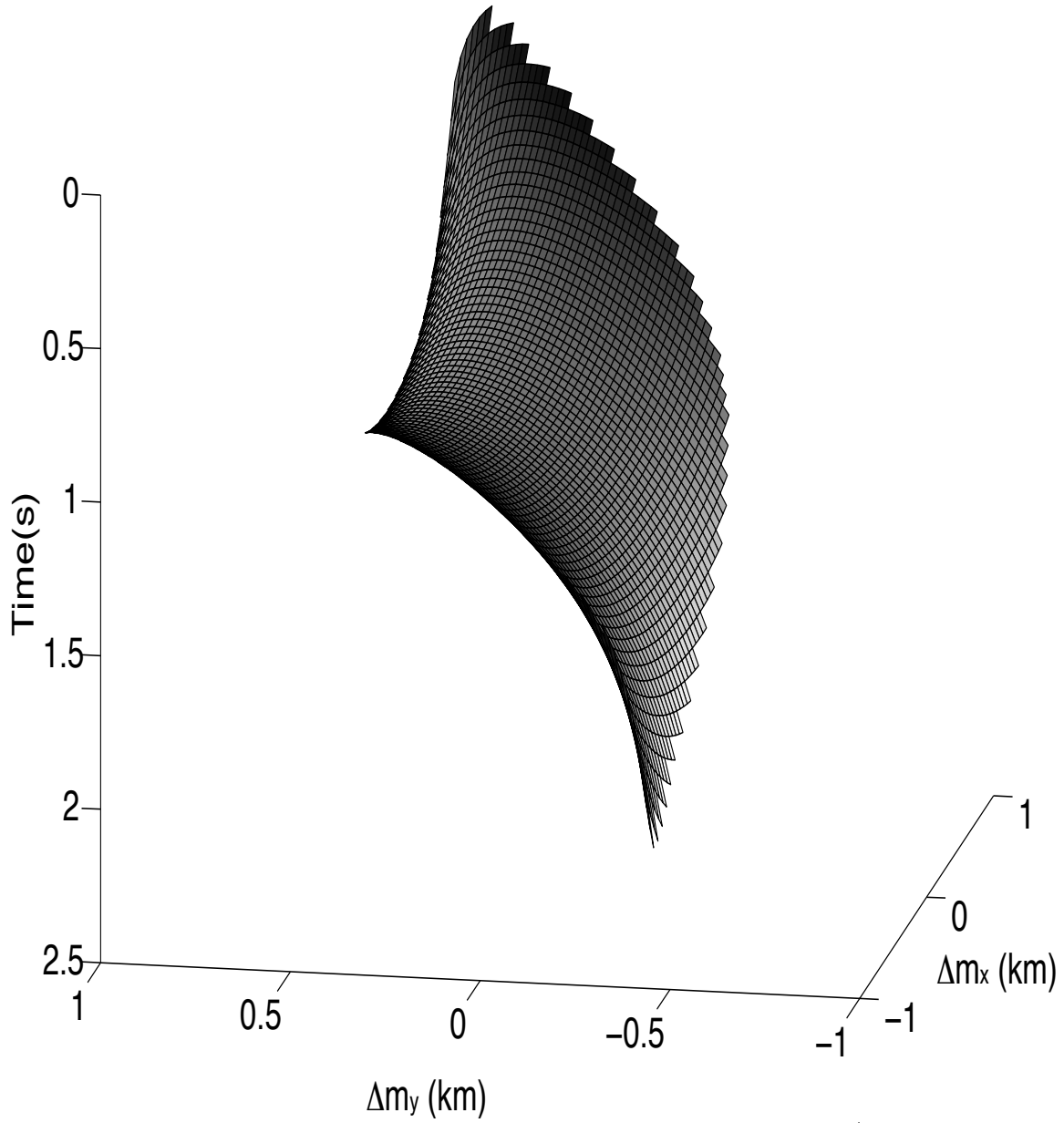


FIG. 3. The effective AMO impulse response when $V_{min} = 2$ km/s, and $t_1 = 1$ s, $h_1 = 2$ km, $h_2 = 1.8$ km, $\theta_1 = 0^\circ$, $\theta_2 = 30^\circ$. Compare with Figure 1.

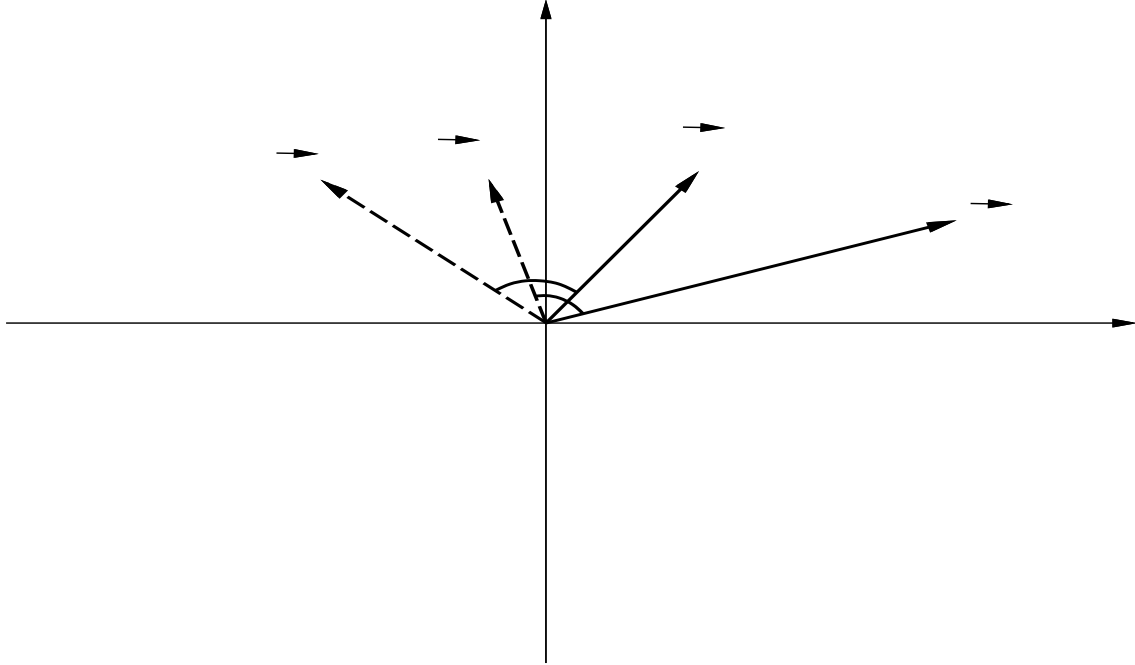


FIG. 4. The geometric relationship between the unit vectors ξ_1 and ξ_2 of the transformed midpoint-coordinate axes, and the input offset \mathbf{h}_1 and the output offset \mathbf{h}_2 .

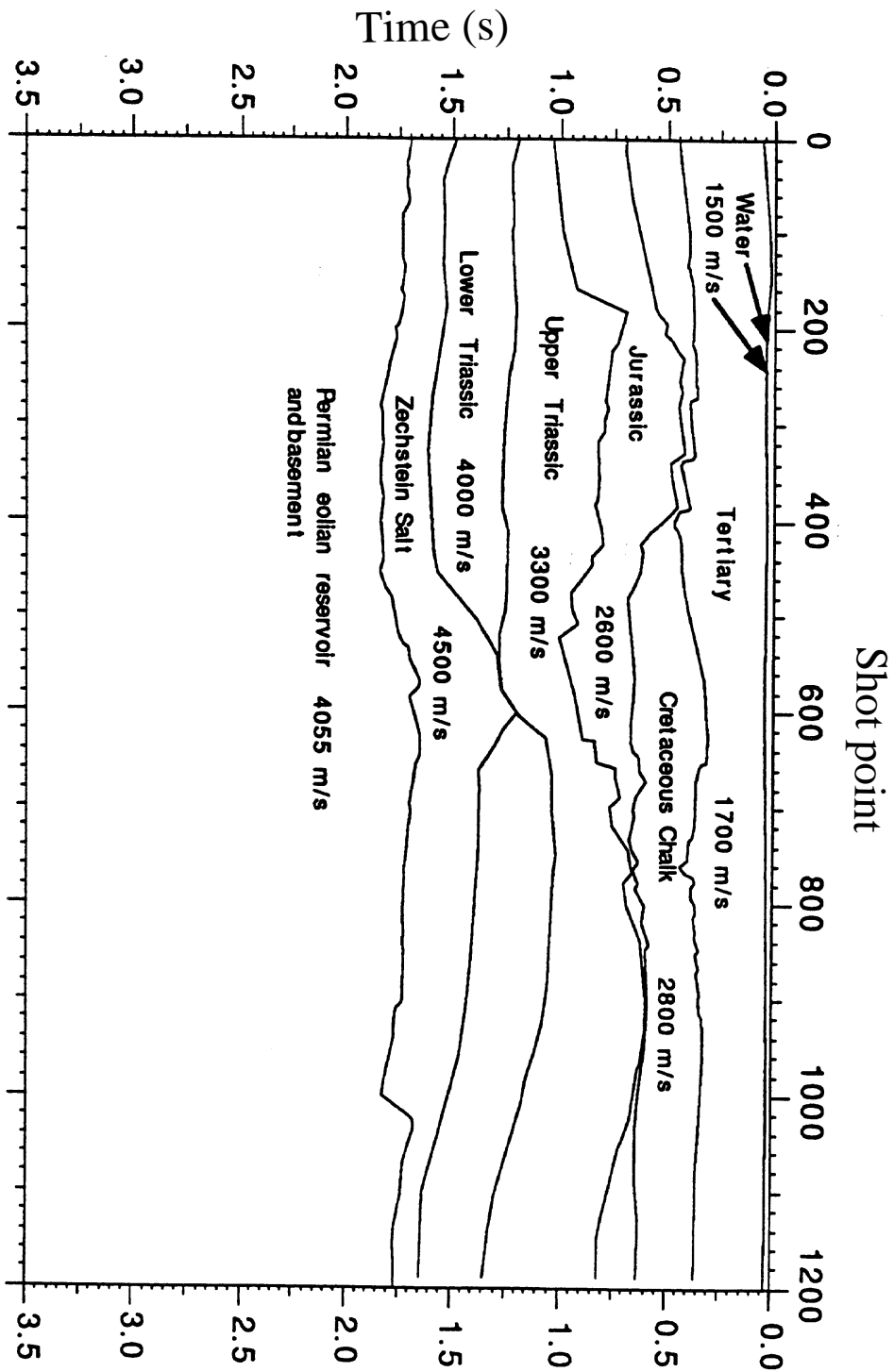


FIG. 5. Geological in-line section and corresponding velocities of layers. From (Hanson and Witney, 1995).

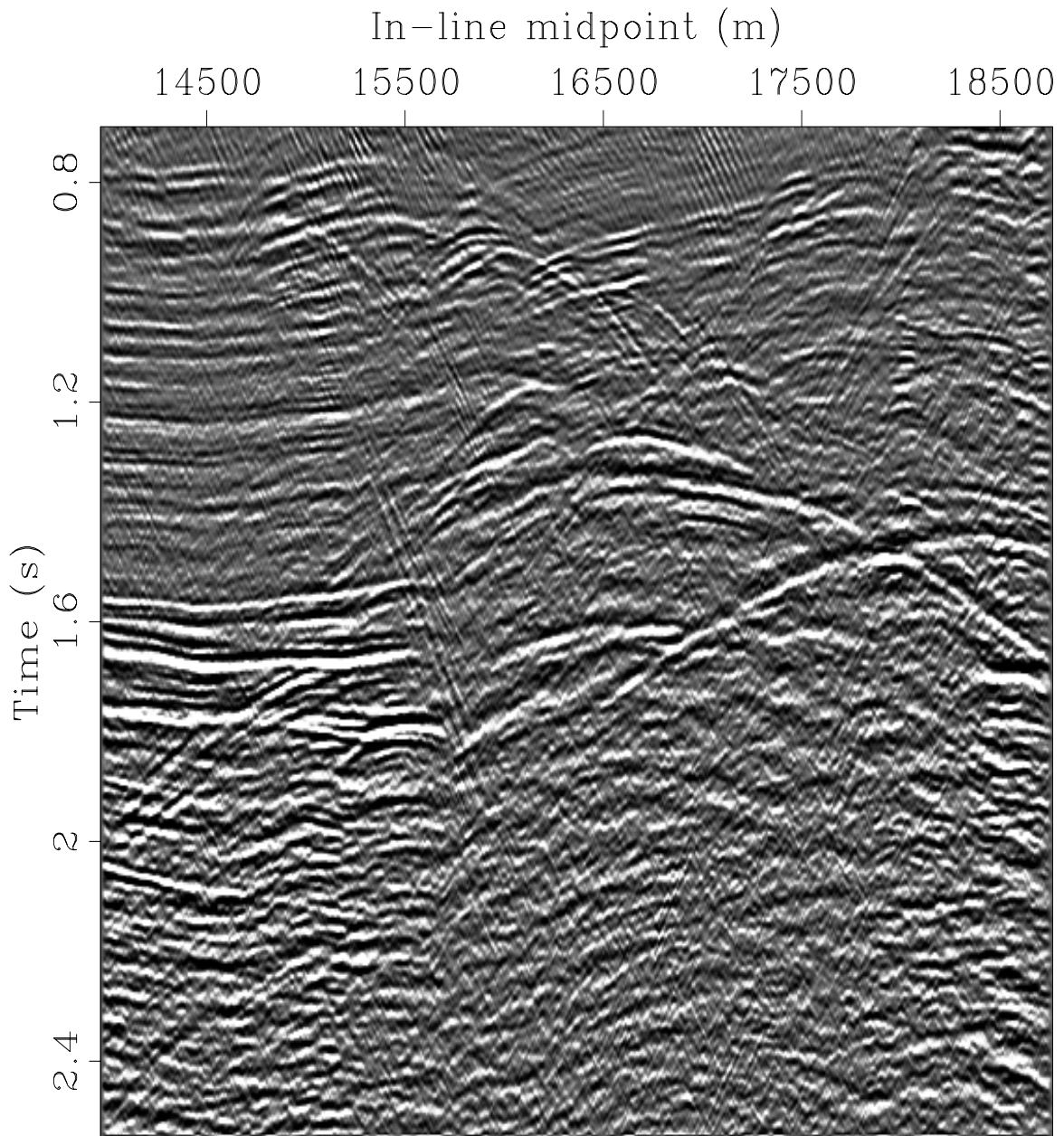


FIG. 6. In-line section of the North Sea data set used for testing AMO.

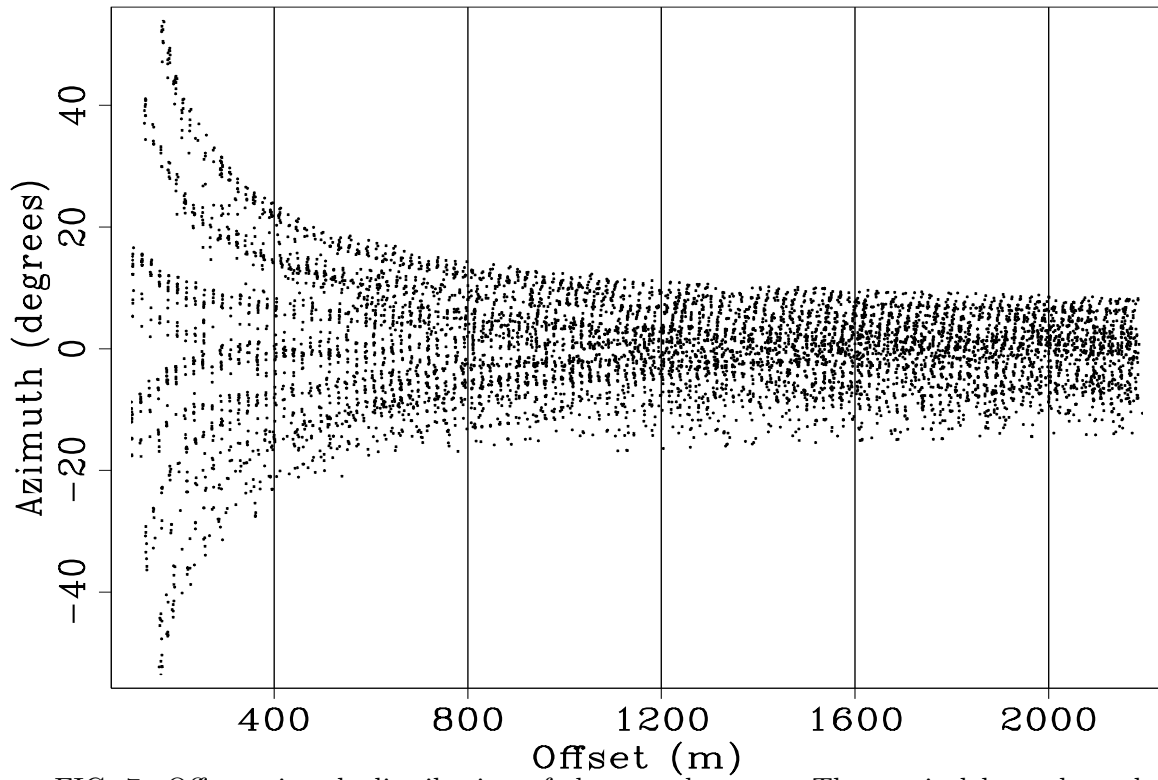


FIG. 7. Offset-azimuth distribution of the test data set. The vertical bars show the boundaries among the offset ranges that were used for partial stacking.

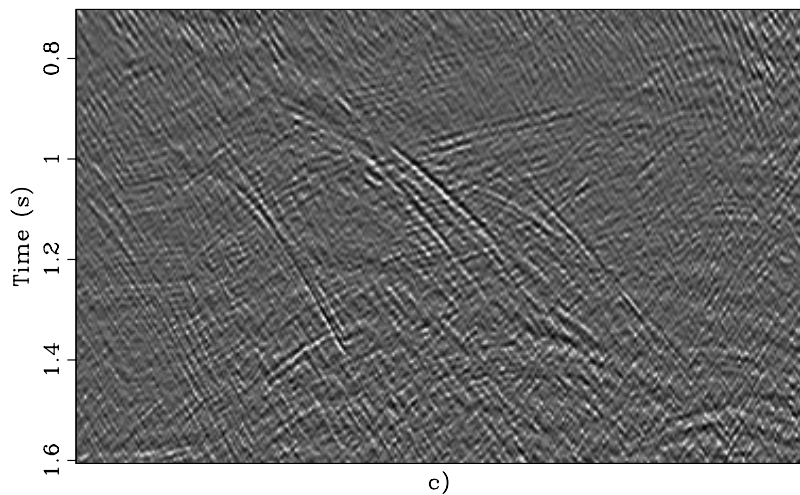
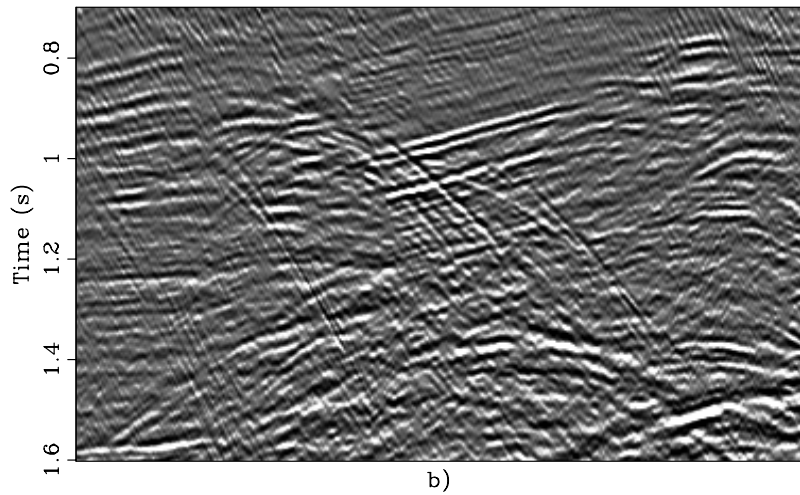
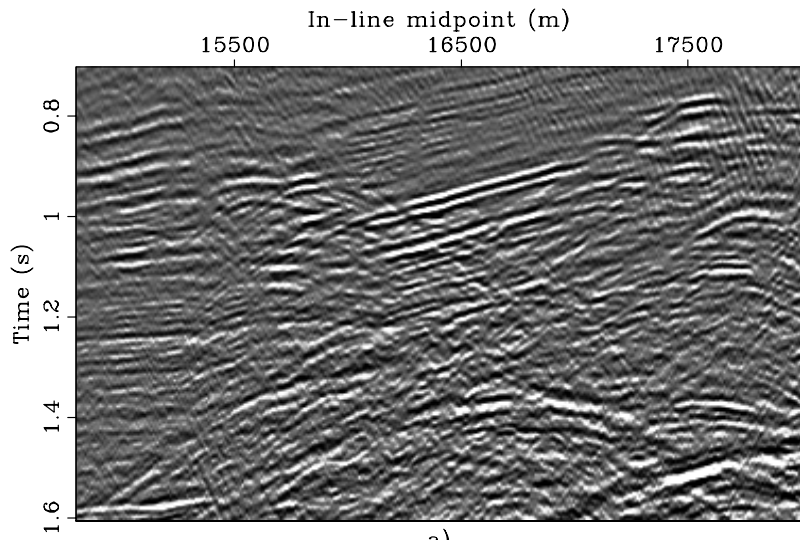


FIG. 8. In-line sections (19,590 m) for the 800 – 1,200 m offset range, obtained by a) NMO-stacking, b) NMO-AMO-stacking, c) subtracting a) from b).

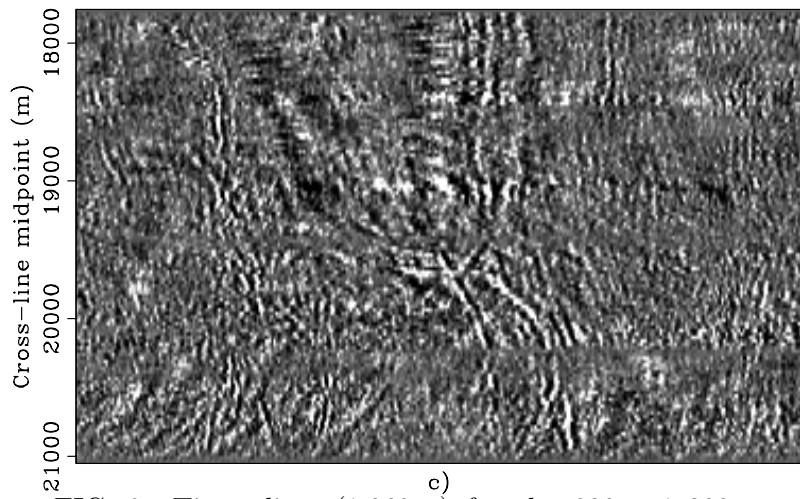
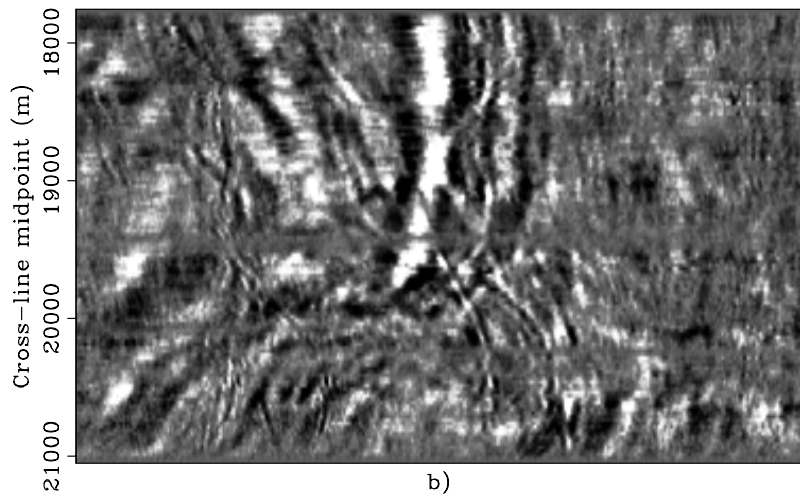
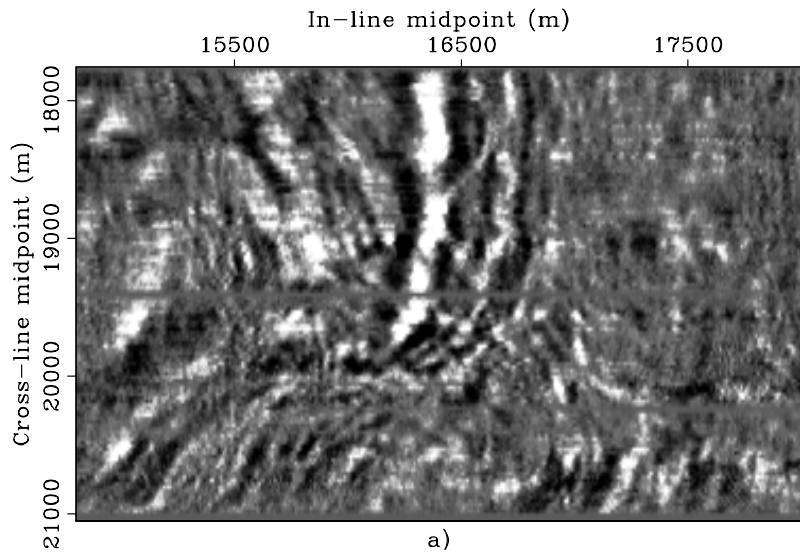


FIG. 9. Time slices (1.068 s) for the 800 – 1,200 m offset range, obtained by a) NMO-stacking, b) NMO-AMO-stacking, c) subtracting a) from b).

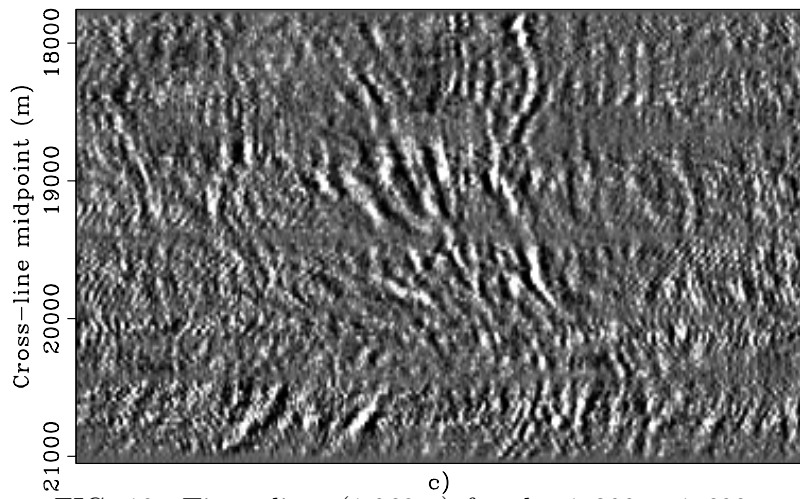
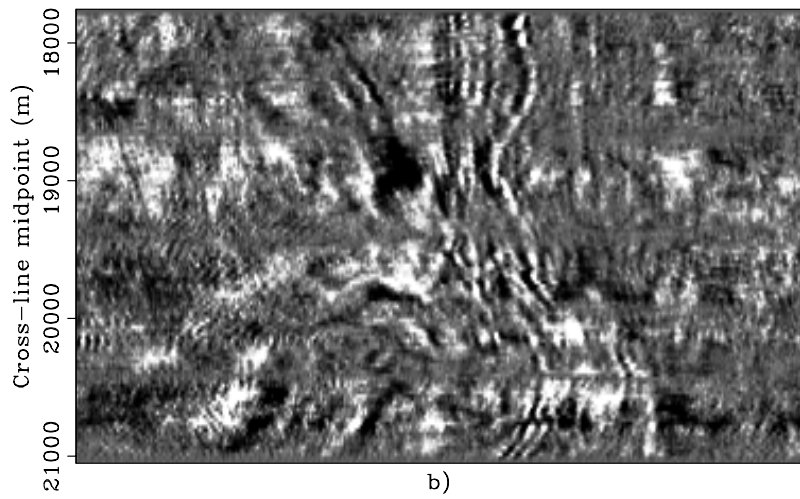
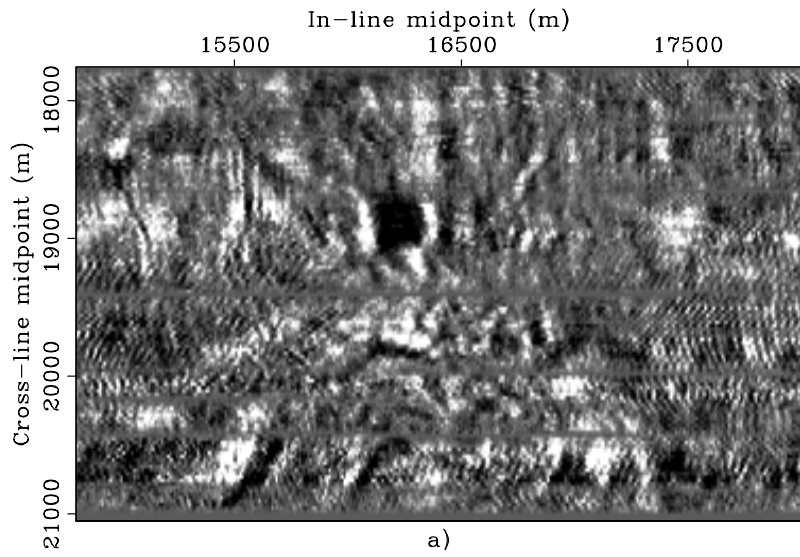


FIG. 10. Time slices (1.068 s) for the 1,200 – 1,600 m offset range, obtained by a) NMO-stacking, b) NMO-AMO-stacking, c) subtracting a) from b).

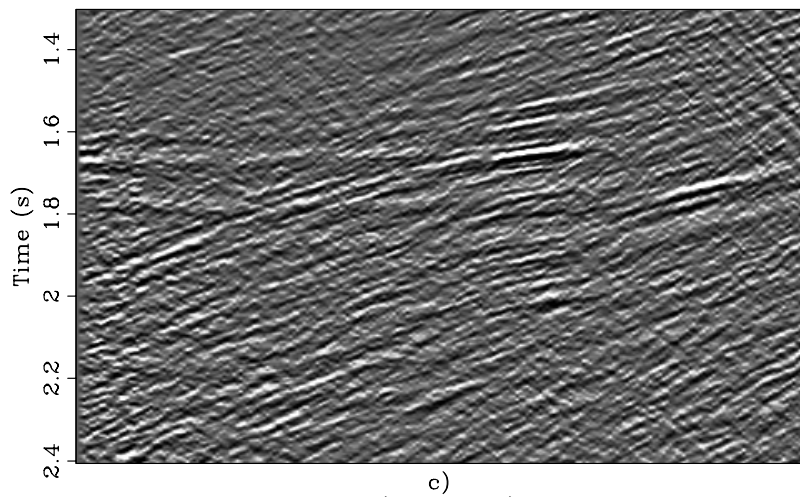
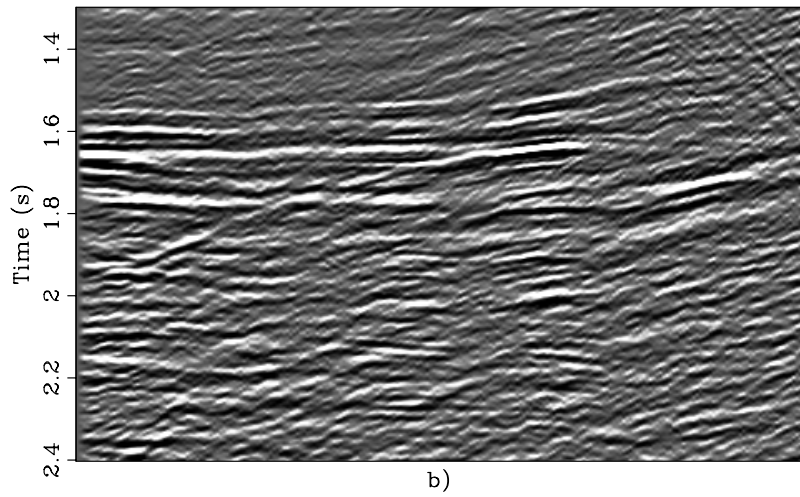
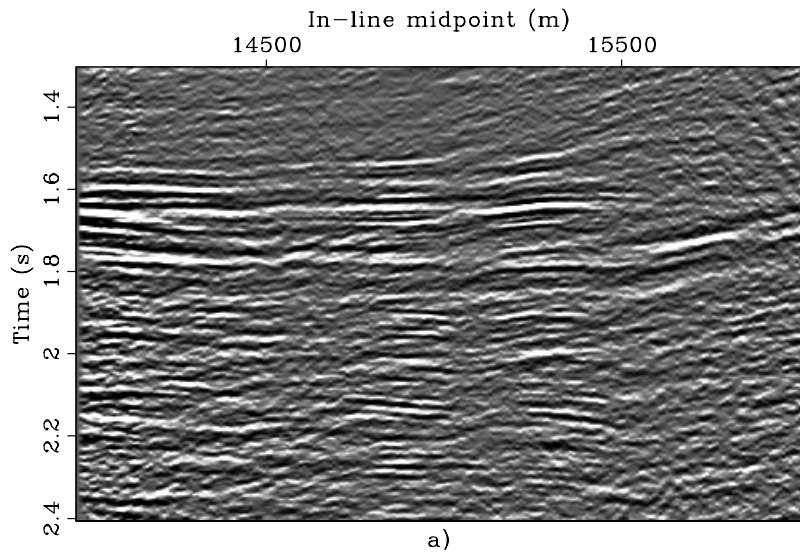


FIG. 11. In-line sections (20,940 m) for the 1,200 – 1,600 m offset range, obtained by a) NMO-stacking, b) NMO-AMO-stacking, c) subtracting a) from b).